University of Stavanger

SCIENCE AND TECHNOLOGY

MASTER THESIS

Curriculum: Petroleum Engineering	Spring semester, 2019 Choose an item.
Author: Luis Jose Abaunza Duran	 ..... (author signature)
Tutors: Merete Madland, Van T.H Pham, Eva Halland, Fridtjof Riis	
Master thesis title: CO_2 Plume Migration in the Stø Formation: A simulation study	
Keywords: CCS, EOR, MMP, Geological Storage, Trapping Mechanisms	Number of pages: 83 + appendices/other: Number of appendices. Stavanger, June 15/2019 date/year

Acknowledgements

I would like to thank the Norwegian Petroleum Directorate and the National IOR Center for their valuable suggestions and assistance.

Secondly, I would like to thank my family. My mom and my dad for their continuous support during this stage of my carrier. And my sister Andrea for her warm and caring heart. I am very grateful with the Universe for giving me the opportunity of studying.

Abbreviations

CCS: Carbon Capture Sequestration

CCUS: Carbon Capture Utilization and Storage

MMP: Minimum Miscibility Pressure

Sor: Residual Oil Saturation

Sw: Water Saturation

Sg: Gas Saturation

EOR: Enhanced Oil Recovery

Kro: Relative Permeability to oil

Krw: Relative Permeability to water

Krg: Relative Permeability to gas

Pcow: Capillary Pressure oil-water

Pcog: Capillary Pressure oil-gas

MPa: Megapascals

cP: Centipoise

mD: Milidarcy

GtC: Gigatonnes of Carbon

MSm^3: Million Standard Cubic Meters

MRm^3: Million Reservoir Cubic Meters

CONTENT TABLE

FIGURES TABLE

TABLES

EQUATIONS TABLE

1. ABSTRACT

The need for improving the quality of our environment by reducing CO_2 emissions and in the meantime increasing the recovery of hydrocarbons could be a mutually beneficial situation. Therefore, having additional reserves that eventually would be commercialized, can generate additional profits that can be achieved with carbon capture sequestration (CCS). In addition, the companies could have CO_2 tax reduction due to the volume of CO_2 injected in geological formations. Some countries encourage to use this smart solution for controlling emissions in the atmosphere after the Paris agreement of 2016.

The Snøhvit field is located in the central part of the Hammerfest Basin in the Barents Sea and the reservoirs were found in the Stø and Nordmela Formations. The hydrocarbon phase in the Snøhvit main field is largely gas with a 10 to 15-meter-thick oil phase. In 2011, the Stø formation was perforated as a new storage location for carbon dioxide, since then all of the CO_2 from the Snøhvit field has been injected in the water zone of the Stø formation, which is in pressure communication with the gas producers on Snøhvit, with no expected pressure buildup in the injection site.

It is probable that the direction of the CO_2 plume will be towards the west and it is believed that this front can be used to mobilize residual oil, which is abundant in the Realgrunnen subgroup. The purpose of this study is to understand the behavior of the carbon dioxide in the zone of interest by using a reservoir simulation software. Notwithstanding there is uncertainty if it would be a miscible or immiscible flood taking into consideration the relative permeabilities of the CO_2 with the oil. For in future allowing to deliver better alternatives in the study of generating a more efficient recovery.

1.2 INTRODUCTION

In the past few years Carbon Capture Sequestration (CCS) has been viewed as a reliable solution for emissions control in the atmosphere. CO_2 storage in the Snøhvit field started in 2008, and at first, it was injected in the Tubåen formation which is dominated by fluvial sandstones. In 2011, due to a fast pressure build up, the injection in the Tubåen formation was stopped, and the shallower Stø formation was perforated as the new geological structure for storage.

In contrast to Tubåen, the Stø formation is in pressure communication with the gas producers on Snøhvit and no significant pressure build-up is expected in the injection site. The hydrocarbon phase in the Snøhvit main field is largely gas and condensate with an oil leg of about 10 to 15 meters. Thick packages of shale seal the Stø formation and are expected to prevent vertical leakage of carbon dioxide. This enhanced oil recovery technique can be used to mobilize residual oil, which is abundant in the Realgrunnen subgroup, allowing to incorporate possible reserves to proven reserves, generating a reduction in costs with the additional recovery of oil, taking into account the greenhouse effect mitigation.

2. THEORETICAL BACKGROUND

2.1 CO_2 Enhanced Oil Recovery Process (CO_2 -EOR)

Soon after an oilfield is discovered, it is developed and produced using primary recovery mechanisms where the reservoir energy drives the hydrocarbon fluids from the underground to the wellbores with pressure decline and consequently starting fluid production. For primary recovery, the range lies between 5 and 20 percent of the original oil in place (OOIP) (Stalkup, 1984, p. 204). Due to these low recoveries, field operators seek to find ways to improve recovery through the application of secondary recovery methods, providing additional energy to the reservoir. Secondary recovery methods involve injecting water and/or natural gas into the reservoir for repressuring it and/or pressure maintenance, in addition to potentially act as a water and/or gas drive to displace oil. This helps to extend the productive life of the reservoir and sustain higher production rates. Normal practice has been to inject water below the oil water contact and inject natural gas into the gas cap or at the top of the reservoir (Verma, 2015, p. 2). Oil recovery at the end of primary and secondary recovery phases are generally in the range 20-40 percent of the OOIP, though in some cases, recoveries could be higher or lower (Stalkup, 1984, p. 204).

After secondary recovery, a substantial amount of residual oil remains in the reservoir and therefore becomes the target for additional recovery using tertiary recovery methods or enhanced oil recovery (EOR) (Verma, 2015, p. 2).

Van Poolen and Associates (1981) classified into three categories EOR methods as the following:

1. Thermal methods, which include steam flood, steam stimulation and in-situ combustion.
2. Chemical methods, which include caustic flooding, polymer flooding, and surfactant polymer injection.
3. Miscible displacement methods, which include the injection, under high pressure, of inert gas, hydrocarbon gas, or CO_2.

Immiscible displacement with CO_2 injection, although not mentioned in the above methods classification, it is also used as EOR.

Enhanced Oil Recovery by means of CO_2 has two major advantages (1) additional hydrocarbon recovery and (2) CO_2 storage to reduce atmospheric emissions of CO_2 (Verma, 2015, p. 2). Oil recovery by CO_2 EOR and its effects on certain properties will be the main focus of this part of the chapter.

2.1.2 Properties of Pure Carbon Dioxide

At atmospheric pressure and temperature, CO_2 is an odorless, colorless gas that is about 1.5 times heavier than air. Some physical properties of pure carbon dioxide are as follows:

Critical Volume: V_c= 0.0022 m3/kg

Critical Temperature: T_c= 31.0 ºC

Critical Pressure: P_c= 7.40 MPa

Normal boiling point: n_{BP}= -78.5 ºC (At 1atm pressure)

Specific Gravity to air: S_g= 1.5194 (At 1atm Sgair= 1.0)

Molecular weight: MW= 44.01 g/gmol

At higher than critical conditions, CO_2 is a supercritical state and forms a phase whose density is close to that of a liquid, although the viscosity remains quite low (0.05-0.08 cp). This dense phase can extract hydrocarbon components from oil more easily than gaseous CO_2 and this is the state that is applied to CO_2-EOR. Even though a low CO_2 viscosity value can be detrimental for oil sweep, within the dissolution in the oil, the oil phase viscosity is also lowered, which in turn helps to improve oil recoveries (Verma, 2015, p. 4).

2.1.3 Fundamentals of the CO_2-EOR Process

The CO_2-EOR process recovers oil that remains in the reservoir after primary and secondary recovery by contacting and mobilizing stranded oil through improving the displacement efficiency (E_d) and the volumetric sweep efficiency (E_v) which are discussed in the section *Factors Determining Recovery Efficiency*. The CO_2 injected may become miscible or remain immiscible

with oil, depending on oil properties, temperature and pressure. The miscible CO_2 injection is preferred over the immiscible mode, because of its higher recovery percentage (Verma, 2015, p. 4).

2.1.3.1 Miscible CO_2 Mode

The minimum miscibility pressure or MMP is defined as the pressure at which miscibility occurs. In 1974 Holm and Josendal defined the MMP as the pressure at which more than 80% of the oil in place is recovered at CO_2 breakthrough. Although an oil recovery of at least 90% at 1.2 HCPV (hydrocarbon pore volume) of CO_2 injected is often used as a rule of thumb for estimating (Yellig & Metcalfe, 1980, p. 32). As seen in Figure 1, oil recovery increases rapidly with increasing pressure, but then flattens out when MMP is reached.

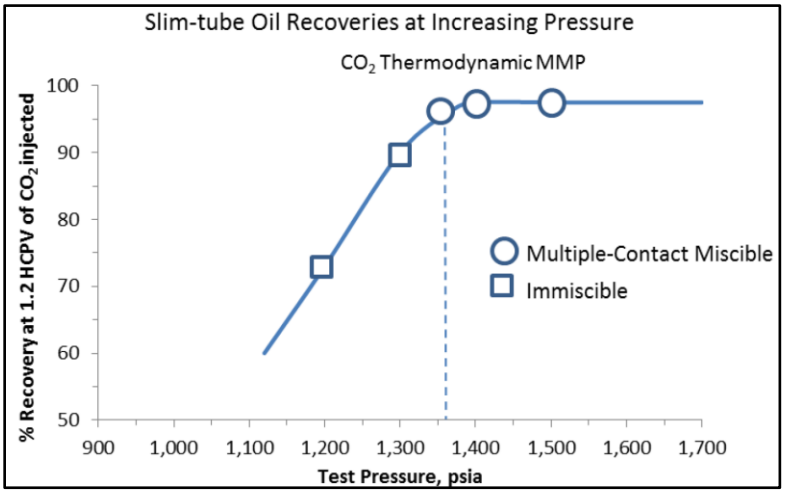

Figure 1. Slim-tube oil recoveries at increasing pressures for fixed temperature and oil composition (from Yellig & Metcalfe, 1980)

Figure 2 shows the relationship between the MMP of CO_2 and several hydrocarbon systems with varying temperature. The temperature is represented in Kelvin (K) and the pressure is represented in Megapascals (MPa) (Lashkarbolooki, M. et al, 2017, p. 121-128).

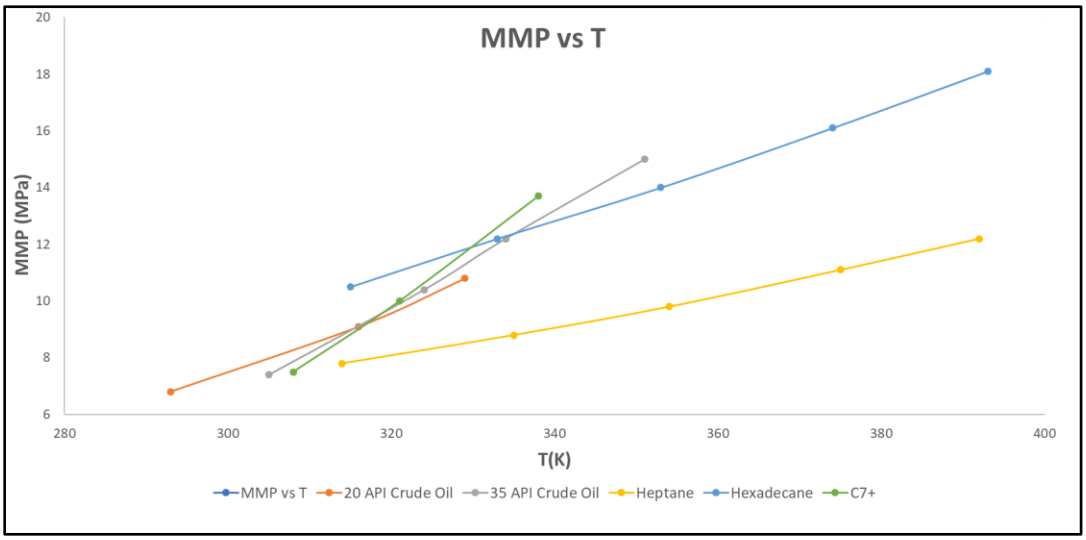

Figure 2. MMP of CO_2 and different crude oils, (Modified from Lashkarbolooki, M., Eftekhari, M., Najimi, S., & Ayatollahi, S. (2017). Minimum miscibility pressure of CO_2 and crude oil during CO_2 injection in the reservoir. The Journal of Supercritical Fluids, 127, 121-128.)

Three types of hydrocarbon miscible mechanisms exist: (1) First contact; (2) Vaporizing gas drive; and (3) the condensing gas drive (Stalkup, 1983, p. 815-826).

(1) First contact miscible solvents mix in all proportions with the reservoir, all the mixture remains in one phase. Carbon dioxide is not miscible on the first contact, but develops miscibility after multiple contacts, which is known as dynamic miscibility.

(2) Dynamic miscibility is achieved by in-situ vaporization of the intermediate molecular weight hydrocarbons from the reservoir onto the injected CO_2.

(3) The condensing gas drive process achieves dynamic miscibility by in-situ transfer of intermediate molecular weight hydrocarbons into the reservoir oil.

As seen in Figure 3, the intermediate and higher molecular weight hydrocarbons from the reservoir oil vaporize into the CO_2 and part of the injected CO_2 dissolves into the oil. This mass transfer between the oil and the CO_2 allows the two phases to become completely miscible without any

interface and helps to develop a transition zone that is miscible with CO_2 in the back and with oil in the front (Jarrel et el, 2002, pg. 220).

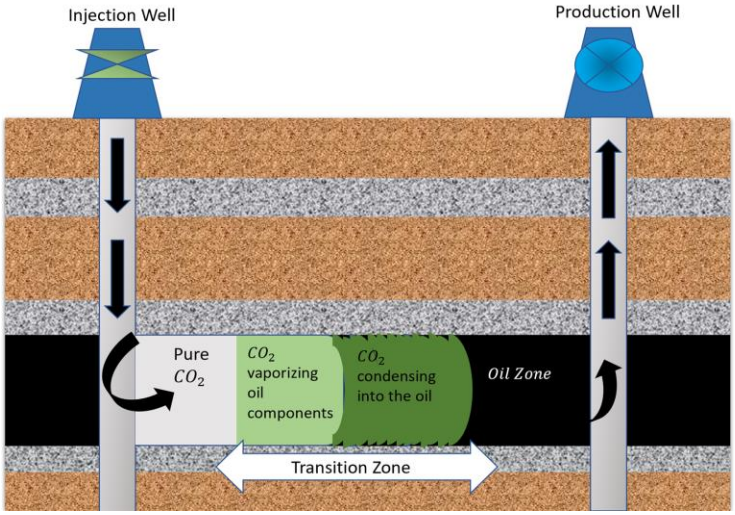

Figure 3. Miscible CO_2 Injection

2.1.3.2 Immiscible CO_2 mode

When the reservoir oil is not favorable or the reservoir pressure is below the MMP, the CO_2 and oil will not form a single phase and thus will not be miscible. However, CO_2 will dissolve in the oil causing viscosity reduction and oil swelling that both help to improve the sweep efficiency and will facilitate additional recovery. CO_2 solubility increases with pressure and decreases with temperature (Simon & Graue, 1965, p. 102-106; Welker & Dunlop, 1963, p. 873). Figure 4 represents this type of process.

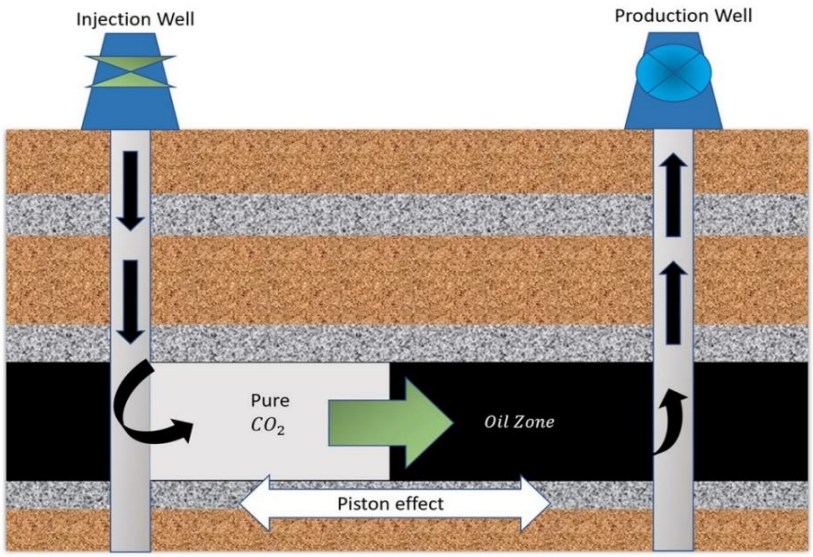

Figure 4. Immiscible CO_2 Injection

2.1.4 CO_2 / Water Injection Strategies

It is not possible for CO_2 alone to displace viscous oils efficiently, thus the CO_2 process must be supplemented with a mobility control mechanism. Some of the most common injection schemes according to Jarrell et al (2002) are:

1. Continuous CO_2 gas injection
2. Carbonated water injection
3. Simultaneous injection of CO_2 gas and water
4. CO_2 gas or liquid slug followed by water
5. CO_2 gas or liquid, followed by alternate water and CO_2 slugs

2.1.4.1 Continuous CO_2 Gas Injection

During this process, carbon dioxide gas is injected continuously until a maximum gas-oil ratio is reached. This process is severely limited in CO_2-heavy oil systems due to lack of gravity and mobility, which are much more present in lighter oil systems as well as reservoirs that are strongly

water-wet or are sensitive to waterflooding. Therefore, sometimes a lighter gas, such as nitrogen, follows the CO_2 injection, to maximize gravity segregation (Verma, 2015, p. 9).

2.1.4.2 Carbonated Water Injection

Carbonated waterflooding was the first method attempted to inject CO_2 into the reservoir. It is shown in Figure 5. In this process, CO_2 diffuses out of the injected water-CO_2 mixture when it contacts the reservoir oil. An effective carbon dioxide concentration at the displacement is not present, because the diffusion process is slow relative to injecting pure carbon dioxide, thus. Due to the extremely low rate of oil viscosity reduction, adverse mobility ratios will continue to exist (Verma, 2015, p. 10).

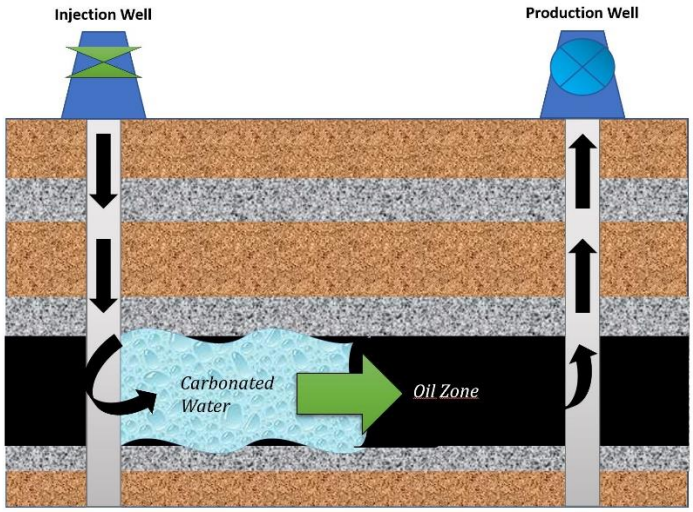

Figure 5. Carbonated Water Injection

2.1.4.3 Simultaneous Injection of CO_2 and water

Warner et al (1977) conducted simulation studies of various carbon dioxide injection strategies. He found that simultaneous injection of CO_2 and water yielded the highest oil recovery. But some major problems may exist with this process. First, the high completion and operating cost for dual injection systems. Secondly, reduced injectivity associated with the injection of two different phases, i.e. gas and liquid. Third, severe corrosion of the injection facilities, due to the acidic nature of carbon dioxide-water systems, reducing equipment life significantly. The process is exemplified in Figure 6 (Farouq Ali, 1992, p. 18-19).

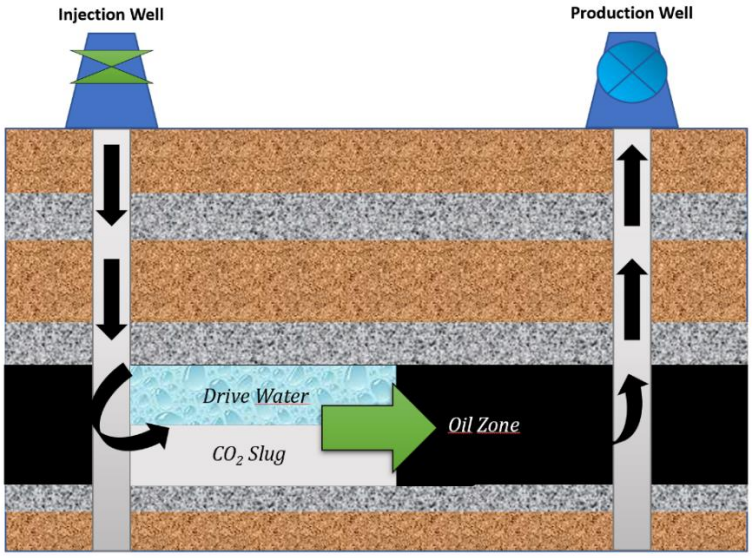

Figure 6. Simultaneous Injection of CO_2 and Water

2.1.4.4 CO_2 slug followed by water

In the CO_2 slug process, a single slug is injected and then followed by continuous water injection to drive the slug through the reservoir, like presented in Figure 7. Additional chase fluids, such as water, are needed to control the lack of gravity and mobility control. This process works well in reservoirs of low permeability and/or moderately homogeneous reservoirs (Verma, 2015, p. 10).

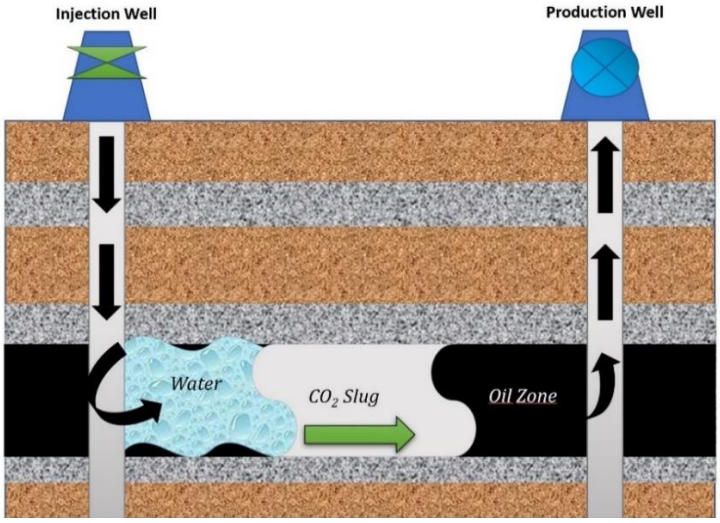

Figure 7. CO_2 slug followed by water

2.1.4.5 Water-Alternating-Gas Process (WAG)

In this process (Figure 8) alternate slugs of CO_2 and water are injected until the desired volume of CO_2 gas and water are injected until the desired volume of CO_2 has been achieved. The process is then followed by a waterflood to further displace the swollen, lower viscosity crude. The WAG ratio of the total volume of water injected to the total volume of CO_2 injected at reservoir conditions. The single slug process may be visualized as having a WAG ratio of zero, while a waterflood may be visualized as an infinite WAG ratio of zero. It has been found the WAG process successfully reduces the mobility ratio and promotes a more uniform distribution of CO_2 throughout the reservoir. Simulation studies conducted by Warner et al (1977) showed that although the WAG process did not recover as much oil as the simultaneous injection processes, it was economically more favorable and recovered more oil than the single and continuous CO_2 processes (Farouq Ali, 1992, p. 19).

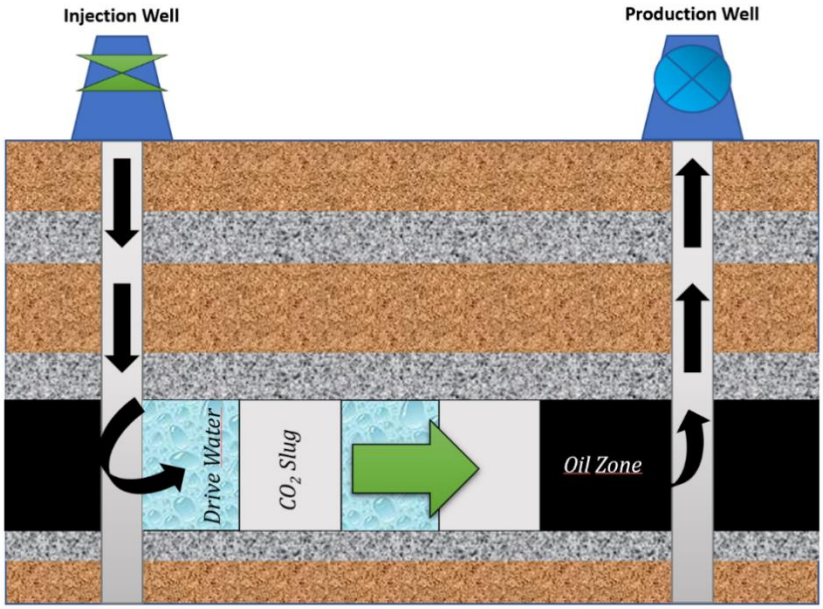

Figure 8. CO_2 slug followed by water

2.1.5 Factors Determining Recovery Efficiency

The total efficiency of any recovery method may be broken down into a combination of individual process efficiencies. And various techniques of enhanced oil recovery aim to improve some or more of the efficiencies shown below. (Farouq Ali, 1992, p. 13).

The equation of overall recovery efficiency is the following.

Equation 1

$$E_R = E_A * E_V * E_D * E_M$$

Where,

$E_R = Overall\ Recovery\ Efficiency$

$E_A = Areal\ Sweep\ Efficiency$

$E_V = Vertical\ Sweep\ Efficiency$

$E_M = Mobilization\ Efficiency$

$E_D = Displacement\ Efficiency$

2.1.5.1 Displacement Efficiency

Defined as the fraction of mobile oil in the swept zone that has been displaced. Displacement efficiency is a function of fluid viscosities, of the relative permeabilities, and the volume of fluids injected. It is the displacement in the swept zone only, and is thus constant until breakthrough. The increases in recovery before breakthrough are due to increasing volumetric sweep $[E_A * E_V]$. (Verma, 2015, p. 12).

The following equation is used to quantify the displacement efficiency, as a function of the fluid injected.

Equation 2

$$E_D(PV_i) = \frac{S_{oi} - S_o}{S_{oi} - S_{res}}$$

Where,

$S_{oi} = Initial\ Oil\ Saturation$

$PV_i = Pore\ volumes\ of\ fluid\ injected$

$S_{orp} = Ultimate\ Residual\ Oil\ Saturation$

Equation 3

$S_o = 1 - S_w = Average\ oil\ saturation\ in\ the\ swept\ zone$

Therefore, it can be seen from the above equation, that improved displacement efficiency is a result from a decrease in oil saturation and/or increased ultimate residual oil saturation (Farouq Ali, 1992, p. 13-14).

2.1.5.2 Mobilization Efficiency

Mobilization efficiency is the fraction of oil in place that ultimately could be displaced by a given process, as defined by Klins (1984). Mobilization efficiency is governed primarily by the ratio of capillary to viscous forces and interphase mass transfer, its independent of the volume of fluid injected. The succeeding equation quantifies the mobilization efficiency.

Equation 4

$$E_M = \frac{S_{oi}/B_{oi} - S_{orp}/B_{of}}{S_{oi}/B_{oi}}$$

Where,

$S_{oi} = Initial\ Oil\ Saturation$

$B_{oi} = Initial\ oil\ volume\ factor$

$S_{orp} = Residual\ oil\ to\ a\ given\ process$

$B_{of} = Final\ oil\ formation\ volume\ factor$

As can be seen from the equation above, improved mobilization efficiency results from a decrease in residual oil and or increase on the final formation volume factor. By reducing the residual oil saturation, blowdown recovery increases mobilization efficiency (Farouq Ali, 1992, p. 16).

2.1.6 Transport of CO_2 in Oil and Reservoir Water

This section has to do with how carbon dioxide mixes with the reservoir fluids. There are three mass transfer mechanisms that affect carbon dioxide transport. Solubility is the most important, diffusion and dispersion also have an effect, to a lower amount.

2.1.6.1 Solubility

CO_2 solubility is one of the most important properties of oil-carbon dioxide systems. As definition, solubility of one substance in another depends fundamentally upon the ease with which two molecular species are able to mix. The property is a strong function of pressure and to a lesser extent of oil composition and temperature. Solubility increases with pressure and reduces with decreased API gravity and temperature (Farouq Ali, 1992, p. 3).

In 1926, Beecher and Parkhurst found that CO_2 was more soluble, on a molar basis, in a 30.2 API oil than in natural gas (CH_4) and air. Further studies done by Holm and Josendal (1974) presented that CO_2 solubility was reduced with increased concentrations of methane and nitrogen. Saxon et al (1951) found that when the bubble point pressure of crude oil increased, carbon dioxide solubility decreased, thus requiring higher carbon dioxide injection pressures. When simulating methane impurities in recycled carbon dioxide gas for the "huff-n-puff" process, Savegh and Maini (1984) also confirmed the reduction in solubility due to methane gas.

Opposite to the findings of Savegh and Maini (1984) and Saxon et al (1951), Chung and Burchfield (1987) hypothesized that as more CO_2 is injected, the solubility of CO_2 would gradually increase in crude oils at reservoir conditions. They theorized that CO_2 would strip the solution gas from the oil causing the methane to be released. Studies done by Zhu et al (1986) of experimental displacement on a scaled physical model compared carbon dioxide and nitrogen. It was found that using nitrogen for oil recovery was similar to that of a waterflood. Residual oil displacement experiments with nitrous oxide and carbon dioxide conducted by Oyekan et al (1983), showed that nitrous oxide, a more powerful solvent than CO_2, recovered more residual oil but the process was highly uneconomical due to its cost.

The solubility of carbon dioxide in water is a function of temperature, pressure and salinity. CO_2 is soluble in water but to a lesser level than in crude oils. Data presented by Dodds et al (1956) shows that for pressures below 10 MPa and in the temperature range of 20-70 ºC, the solubility of carbon dioxide in fresh water, is less than six percent by weight. Stewart and Munjal (1970) carried out CO_2 solubility experiments in synthetic sea water and discovered that CO_2 solubility was reduced with increasing temperature and salinity. Klins et el (1984) noted the solubility of carbon dioxide in water must be accounted for projects undergoing tertiary recovery.

2.1.6.2 Diffusion

Diffusion is independent of any convection within the system, and in other words, is the macroscopic transport of mass, due to random molecular motion. CO_2 mixes well with oil by diffusion and by solution. Diffusion is not related to the attractive forces as measured by solubility. A rise in temperature reduces solution, yet enhances diffusion, because of the increasing molecular

motion. While solution, is by definition, the amount of dissolved solvent at equilibrium, diffusion is a rate process under non-equilibrium conditions. Molecular diffusion has shown to be an important rate controlling mechanism in CO_2 floods and is responsible for a mass transfer at the pore level. This phenomenon helps carbon dioxide penetrate in the oil which may allow to reduce viscous and gravitational instabilities (Farouq Ali, 1992, p. 5). Literature data indicate that the diffusion rate of carbon dioxide in water is greater than the diffusion rate of carbon dioxide in oil. As found by Denoyelle and Bardon (1984), the diffusion of CO_2 in a liquid (oil and water) proceeded at an intermediate rate that in oil alone or in water alone. They pointed out that due to the pore scale being so much larger than the molecular scale, the porous medium has a negligible effect on molecular diffusion.

2.1.6.3 Dispersion

Velocity is responsible for additional mixing of fluids in the porous medium. This additional mixing is due to the fact that hydrocarbons by being highly polarizable molecules, exert a dispersive force of attraction. However moderate velocities are encountered at reservoir conditions; therefore, transport of carbon dioxide is less influenced by convective dispersion than by molecular diffusion (Farouq Ali, 1992, p. 6).

2.1.7 Effects of CO_2 on Oil, Water, and Formation Properties

The formation fluids and the rock may go through dramatic changes when exposed to CO_2. Reduction in oil viscosity is the most notable of these changes. This section describes what happens in the reservoir when injecting CO_2 into the formation.

2.1.7.1 Viscosity Reduction

CO_2 is approximately fifty percent heavier than air at atmospheric conditions, making it a relatively dense gas. The viscosity of carbon dioxide gas is a strong function of pressure and temperature.

According to Godrich et al (1980), CO_2 gas viscosity decreased to a lesser extent with temperature and increased significantly with pressure. Carr et al (1959) conducted several experiments at atmospheric conditions, and they evidenced that at any given temperature CO_2 is more viscous than methane, ethane, propane and hydrogen sulphide but less viscous than nitrogen and air. Hence, the viscosity of pure carbon dioxide gas at 10 bar and 20.6 ºC is approximately 0.022 cP.

The most important effect of CO_2 on crude oil systems is the notable viscosity reduction. The viscosity of oil saturated with carbon dioxide is a function of temperature, pressure and concentration of dissolved carbon dioxide. It has been found by a number of researchers that large percentage reductions in viscosity occur at lower operating temperatures. As noted by Killesreiter (1982), at temperatures above 145 ºC, the effect of dissolved CO_2 on oil viscosity was negligible. Jacobs et al (1978) conducted experiments on Athabasca bitumen, showing that due to carbonation, the most dramatic decreases in viscosity took place at temperatures below 100 ºC. The reason for this was the increased CO_2 solubility at lower temperatures. The work done by Rojas and Farouq Ali (1985a) indicated that the higher the initial oil viscosity, when saturated with subcritical CO_2, the greater the percentage reduction in viscosity. They reported a 95.6 percentile decrease in viscosity for a 1080 cP oil and a 98.3 percentile decrease in viscosity for a 4900 cP oil, having the samples saturated at 55 bar and 21 ºC with subcritical CO_2. They also noted that these reductions in viscosity, by CO_2 saturation, were comparable to heating the oil samples to approximately 90 ºC.

2.1.7.2 Density Change

Holm and Josendal (1974) also noted that CO_2 has a surprising effect on the density of crude oil. Opposite to what one may expect, the density of crude oil increases as it becomes saturated with carbon dioxide.

2.1.7.3 Interfacial Tension Reduction

In 1926, Beecher and Parkhurst conducted experiments to determine the interfacial tension between crude oils and gases. The results obtained showed a reduction in the surface tension of crude oils

of approximately 20%. Rojas and Farouq Ali (1985a) found that interfacial tension decreases moderately with increasing carbonation pressure of brine. The interfacial tension was reduced from approximately 25 to 16 mN/m when the pressure was increased from 0.1 to 5.5 MPa). The reduction in interfacial tension, as noted by these authors, may be due to the action of carbonic acid on the nitrogen bases, found in the Lloydminster Aberfedy crude oil. The formation of surfactants would then concentrate at the oil-water interface. Martin (1951) suggested that the CO_2 bonds chemically with these nitrogen bases to form polar compounds, which would drastically reduce the interfacial tension of oil-water systems.

The in-situ formation of water in oil emulsions, due to concentrated surfactants at the oil-water interface were described by Rojas and Farouq Ali (1985b) as the mechanisms of in situ emulsification, during immiscible displacement of oil by carbon dioxide as follows:

1. The reduction in interfacial tension between the oil and the acidic brine breaks down the droplets into smaller and more stable brine droplets.
2. In the swollen carbonated oil Fingers of formation water lead to the formation of large brine droplets inside the oil.

After brine breakthrough in scaled model displacement experiments, Rojas (1985) observed the production of viscous gasified emulsions.

2.1.7.4 Asphaltene Flocculation

When crude oil and CO_2 mix, multiple liquid phases may exist in equilibrium. asphaltene precipitates deposition can create serious problems in the reservoir, such as injectivity problems associated with wettability reversal or constriction of fluid flow passages. This asphaltene precipitation occurs when the hydrocarbons and polar fractions lose their ability to colloidally disperse the asphaltene fraction. There are several factors that can influence asphaltene flocculation like: temperature, pressure, crude oil composition and properties of the asphaltenes. Throughout the years asphaltene flocculation experiments with light oils have shown that the extent of carbon dioxide-induced asphaltene precipitation correlates with temperature and temperature as they relate to the development of miscibility (Farouq Ali, 1992, p. 11-12). Bryant and Monger (1985) phase behavior measurements showed that the development of multi-contact miscibility is related to

extensive asphaltene precipitation. Although due to the findings of Hirschberg et al (1981) it appeared that the asphaltene flocculation is reversible when pressure is reduced.

2.1.7.5 Permeability Changes

Carbonates are present in many formations as they constitute the bulk matrix in dolomite and limestone reservoirs. In sandstone reservoirs, carbonates are often found consolidating the sand grains as cements. The most commonly found carbonates in the reservoir rocks are those of magnesium and calcium (Ross G.D. et al, 1981).

When injecting CO_2 and water, formed carbonated water, will react with the carbonate minerals in the reservoir. Ellis (1959) summarized the chemical process as follows:

1. CO_2 and water are injected into the reservoir and the carbon dioxide in the water forming hydrogen carbonate, which then dissociates to give carbonic acid:

Equation 5

$$CO_{2\,g} \leftrightarrow CO_{2\,aq} + H_2O \leftrightarrow H_2CO_{3\,aq} \leftrightarrow {H_{aq}}^{+} + {HCO^{-}}_{3\,aq}$$

2. The acid then reacts with the carbonate, such as calcite:

Equation 6

$${H_{aq}}^{+} + {HCO_3}^{-} + CaCO_{3\,s} \leftrightarrow {Ca_{aq}}^{2+} + 2({HCO_3}^{-})_{aq}$$

The equilibrium of the above equations can be affected by changes in concentration of reactants and products, temperature and pressure.

Lund and Fogler (1976) suggested that the dissolution occurred at preferred sites such as exposed grains and constrictions. Opposite to Ross et al (1981) that felt the phenomenon of channeling is more likely to be the dominating mechanism leading to increased permeability.

Several investigators, have also noted the negative effects of rock dissolution. Carbonate precipitates and small particles could reduce permeability by blocking pore channels.

2.1.7.6 Viscous Instabilities

The primary purpose of the immiscible CO_2 flooding is to decrease the effective viscosity of the displaced fluid relative to the displacing fluid. The viscosity of CO_2 at 10 bar and 20.6 ºC is approximately 0.022 cP.

The process of immiscible carbon dioxide tertiary recovery may be viewed as oil viscosity reduction, due to carbon dioxide, followed by water immiscibility displacing the reduced viscosity oil (Farouq Ali, 1992, p. 14).

2.1.7.7 Mobility Ratio

Defined as the ratio of displacing phase mobility to the displaced phase mobility. The mobility equation for the displacement of oil is as follows (Farouq Ali, 1992, p. 15):

Equation 7

$$M = \frac{\left({k_{rd}}/{\mu_d}\right)_{displacing}}{\left({k_{ro}}/{\mu_o}\right)_{displaced}}$$

Where,

$k_r = relative\ permeability\ at\ average\ phase\ front$

$\mu = fluid\ viscosity$

The adverse mobility ratio due to large viscosity differences may result in the formation of viscous fingers, especially in crude oils with lower API. This viscous fingering causes drastic reductions in the displacement efficiency and early CO_2 breakthrough. Bernard et al (1980) recognized that injecting water, as a mobility control agent for carbon dioxide floods, may have several negative effects including increased water flow, trapping of oil, and diminished extraction of hydrocarbons by carbon dioxide.

2.1.7.8 In-Situ Emulsion Formation

The reduction in interfacial tension between the displacing phase and oil leads to the formation of a water-in-oil emulsion, as proposed by Rojas and Farouq Ali in 1985. Rheological studies conducted on carbon dioxide-water emulsions by Farouq Ali et al (1988), have shown emulsion viscosity, at atmospheric conditions, is of the order of 7000 cP. These studies indicate that the emulsion forms in thin banks thus improving the mobility ratio without appreciably increasing pressure drop.

2.1.7.9 Blowdown Recovery

Blowdown recovery is the oil recovered upon the termination of a flood by depleting the pressure in the reservoir to a low value. The recovery mechanism is analogous to a solution gas drive. The fluids contain drive energy due to dissolved CO_2 under pressure. As the pressure is reduced, the carbon dioxide in solution expands and drives the fluids from the reservoir. Blowdown recovery decreases the residual oil saturation, therefore increasing the displacement efficiency (Farouq Ali, 1992, p. 16).

2.1.7.10 Capillary Number Effects

The capillary number characterizes the ratio of capillary to viscous forces. The equation for the capillary number is as follows.

Equation 8

$$N_c = \frac{\upsilon\mu}{\sigma} = \frac{k\left(\frac{\Delta p}{\Delta L}\right)}{\sigma}$$

where,

$N_c = capillary\ number\ (dimensionless)$

$\upsilon = displacing\ fluid\ Darcy\ velocity\ (\frac{m}{s})$

$\mu = displacing\ fluid\ viscosity$

$\sigma = interfacial\ tension\ (N/m)$

$$k = absolute\ permeability\ (m^2)$$

The process immiscible CO_2 flooding increases the capillary number by reducing the interfacial tension between the displacing and displaced phases. Permeability may rise due to dissolution of carbonates. These mentioned factors would increase the capillary number by less than one order of magnitude. where complete miscibility is achieved (MMP). Excessively high pressures would be required to increase the pressure gradient $\left[{}^{\Delta p}/_{\Delta L}\right]$ and reduce the interfacial tension to zero (Farouq Ali, 1992, p. 17).

2.1.7.11 Oil Swelling

When contacted with CO_2, crude oils swell. Injection of CO_2 increases the oil formation volume factor artificially and at the end of the injection, the final formation volume factor is significantly increased, henceforth enhancing the mobilization efficiency. Blowdown recovery reduced the formation volume factor B_{of} the oil does not shrink to its original volume. At high pressures B_{of} may also be increased by the components of the oil that get stripped into the vapor phase (Farouq Ali, 1992, p. 17).

2.2 CCS- CARBON CAPTURE AND STORAGE

Carbon capture sequestration is a process that consists of the separation of CO_2 from energy-related and industrial sources, transport to a storage site and isolation from the atmosphere for a long time.

2.2.1 CO_2 Impact on Climate Change

Amongst the science community, it is well accepted that one of the main causes for climate change is due to greenhouse gas emissions. As can be seen from figure 9, the quantity of CO_2 emissions is the highest in comparison to other greenhouse gases like methane and nitrous oxide, with a value of 35.47 billion tonnes in the year 2014. Methane and nitrous oxide presented values of 8.01 billion tonnes and 3.155 billion tonnes respectively (Ritchie H. & Roser, M., 2017).

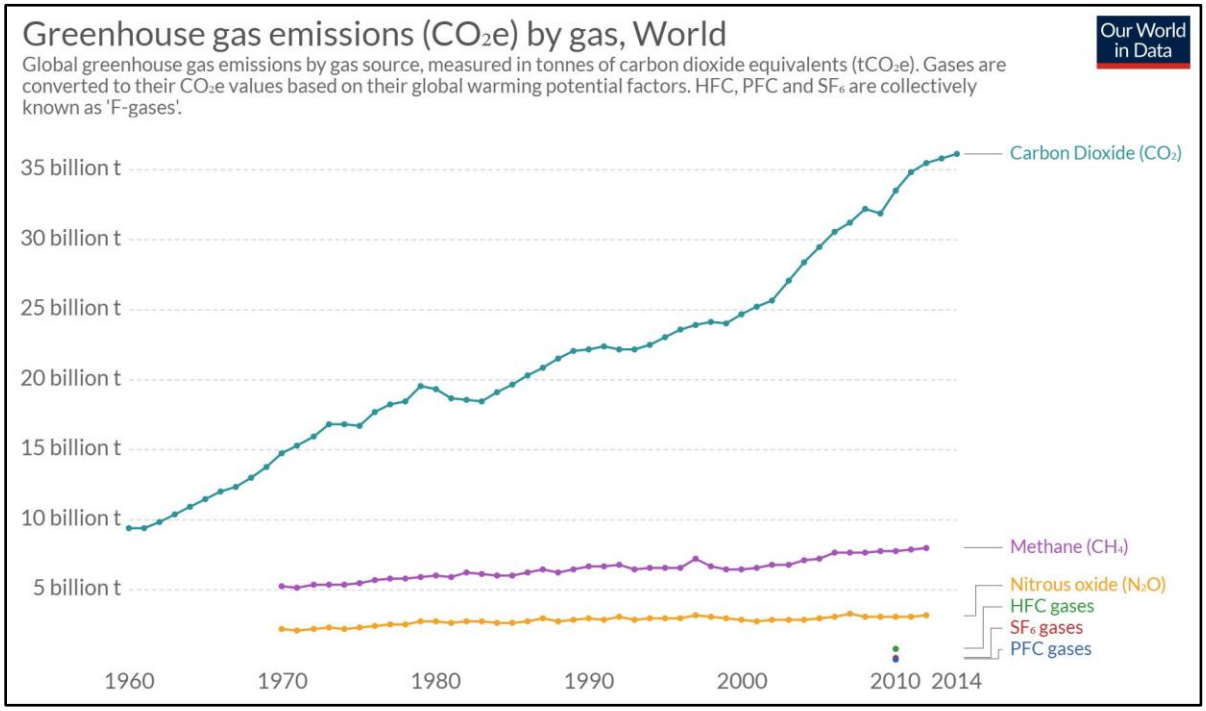

Figure 9. Greenhouse gas emissions in the past years, retrieved from https://ourworldindata.org/co2-and-other-greenhouse-gas-emissions

Figure 10 shows how, since the industrial revolution, the induced temperature change made by humans has increased exponentially. This is evident in the average increase of one degree during

the last 160 years. At this point it is important to raise the question, of what can be done to stop this progression in temperature.

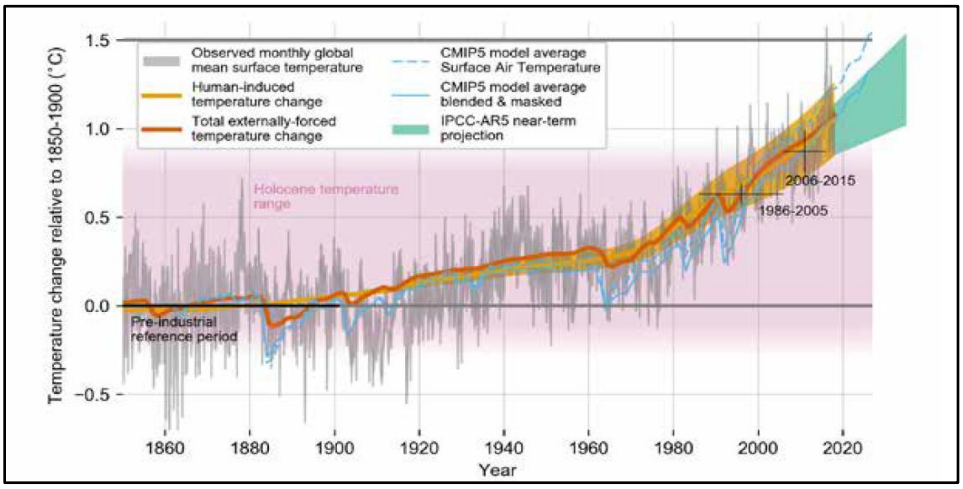

Figure 10. Temperature change relative to 1850-1900 ºC, retrieved from https://twitter.com/valmasdel/status/1051751761738964994

2.2.2 CCS as a solution for mitigating emissions

With the signing of the Paris agreement in 2016 and with the compromise of keeping global temperatures below 2 degree Celsius by the turn of the century, several proposals have been taking into consideration to slow down the process (Page, 2018, p. 3).

As new technology emerges, and with the goal of helping the environment, Carbon Capture Sequestration (CCS) has been seen as a partial solution that can contribute greatly to mitigate emissions. The technology has been applied in some fields of the Norwegian Continental Shelf, having a history of over 20 years of safely storing CO_2 in Sleipner, more exactly in the Utsira formation. CCS has also been applied in Snøhvit where the gas that is produced comes with high amounts of carbon dioxide therefore making it necessary to treat the stream at the plant in Melkøya. Nowadays, there are in operation several applications that through large industrial plants separate CO_2. Carbon dioxide is usually removed to purify other industrial gas streams but this process has been used for storage purposes only a small number of times, in most cases it is released to the atmosphere. Processes involving capture have also been used to obtain commercially right amounts of CO_2 from flue gas streams produced by the combustion of coal or natural gas.

Overall, the main focus of CO_2 capture is to produce a stream of CO_2 at high pressure and concentrated enough, so that it can be suitably transported to a storage site. Energy cost and other associated costs do not allow the entire gas stream containing low concentrations of CO2 to be transported and injected underground, thus making it necessary to produce a nearly pure stream for transport and storage. Even though CCS involves capture, transportation, geological storage, monitoring and verification, in this section, the main focus will be on the geological storage of CO_2 and important ideas regarding monitoring and verification will be mentioned.

On Figure 11 it can be understood where CCS is as of now, showcasing different ongoing projects around the world. Scenario studies indicate that the number of large CO_2 point sources is projected to increase in the future, and that, by 2050, given expected technical limitations, around 20-40% of global fuel CO_2 emissions could be technically suitable for capture, including 30-60% of the CO_2 emissions from electricity generation and 30-40% of those from industry (Metz, 2005, p. 31)

.

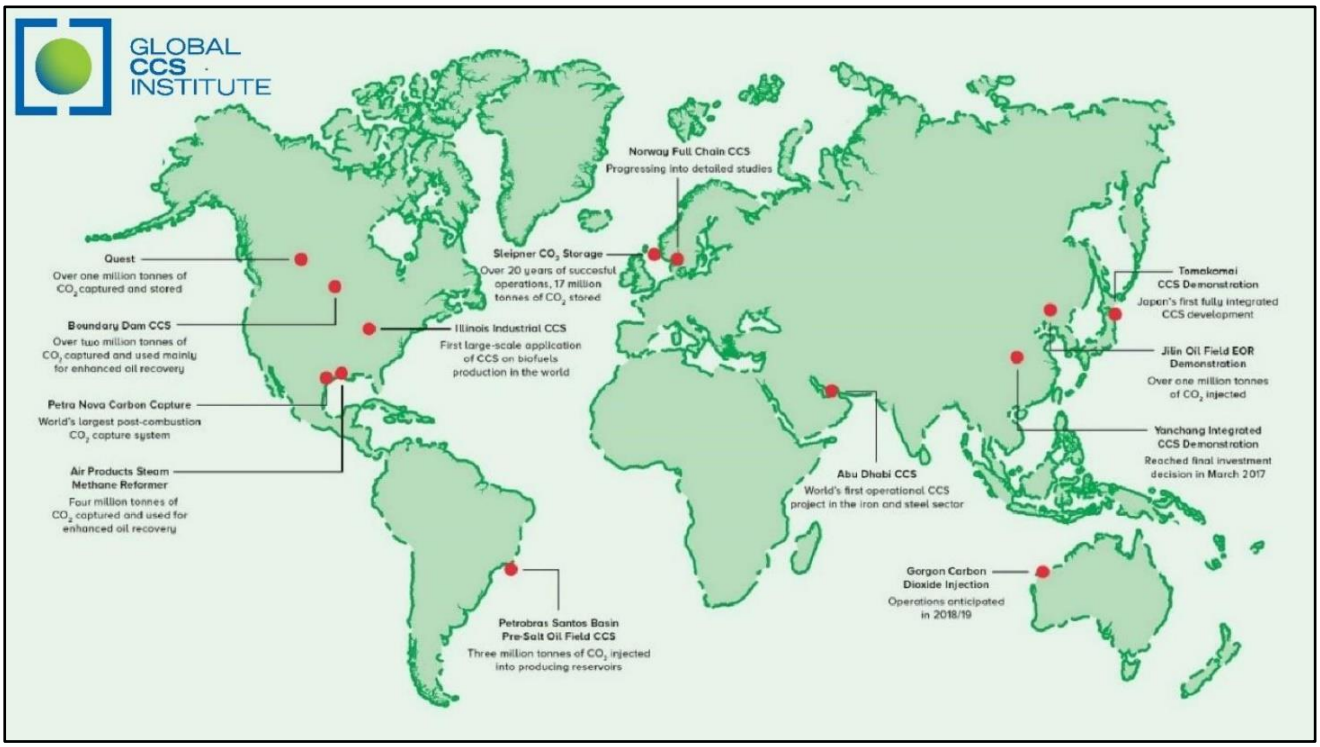

Figure 11. CCS Facility Development Globally, retrieved from https://unfccc.int/sites/default/files/resource/40_UNFCCC%20Submission_Global%20CCS%20Institute.pdf

2.2.3 Geological Storage

Several of the same technologies that have been developed in the oil and gas exploration and production industry have been applied to the injection of CO_2 into deep geological formations. Computer simulation of storage, reservoir dynamics, injection technology, well-drilling technology, and monitoring methods from existing applications are being functional further for design and operation of geological storage.

As shown on Figure 12, there are essentially three types of geological formations that have received widespread attention for storage of CO_2; deep saline aquifers, unminable coal beds and depleted oil and gas reservoirs. By injecting CO_2 in supercritical conditions into a rock formation below the Earth's surface, geological storage is achieved for each case. Porous rock formations that hold or have previously held fluids, such as oil, brines or natural gas are potential candidates for CO_2 storage. If permeability is sufficient, coal beds may also be used for storage when it is highly unlikely that the coal will later be mined. Formations that are suitable for storage can occur in both offshore and onshore sedimentary basins (Metz, 2005, p. 31).

Generally, CO_2 storage is anticipated to take place at depths below 800m, in deep saline aquifers or hydrocarbon reservoirs, where the temperatures and pressures will generally result in CO_2 being in supercritical state. The density of CO_2 will range from 50 to 80% of the density of water under these circumstances. This is similar to the density of some crude oils, resulting in buoyant forces that tend to drive CO_2 upwards. Thus, it is important to have the presence of a well-sealed cap rock over the selected storage reservoir in order to ensure that CO_2 remains trapped underground. During underground injection, the CO_2 compresses and fills the pore space by partially displacing the in-situ fluids, in other words the fluids that are already present in the reservoir. The displacement of the in-situ fluids by injected CO_2 in oil and gas reservoirs can result in most of the pore volume being available for CO_2 storage (Metz, 2005, p. 31).

The fraction retained into the storage formation, depends on a combination of physical and geochemical trapping mechanisms. Above the storage formation a layer of shale and clay rock provides physical trapping to block upward migration of CO_2. This impermeable layer is known as the cap rock. Capillary forces that retain CO_2 provide additional physical trapping in the pore spaces of the formation. Nevertheless, in many situations, one or more sides of the formation

remain open, permitting for lateral migration of CO_2 beneath the cap rock. In these cases, additional mechanisms are important for the long-term entrapment of injected CO_2.

Geochemical trapping is the mechanism that arises as the O_2 reacts with the host rock and the in-situ fluids. Initially, CO_2 dissolves in the in-situ water. This takes place over time scales of hundreds to even thousands of years, and the CO_2-water system becomes denser, hence sinking down into the formation. Afterwards, chemical reactions between the rock minerals and the dissolved CO_2 form ionic species, so that a fraction of the injected CO_2 will be converted to solid carbonate minerals over millions of years. But then again, another trapping mechanism occurs when preferentially adsorbed onto organic-rich shales or coal replacing gases such as methane. Under these circumstances, CO_2 will remain trapped as long as pressures and temperatures remain stable (Metz, 2005, p. 32).

2.2.3.1 Depleted Oil and Gas Reservoirs

One of the main advantages for using depleted oil and gas reservoirs for CO_2 sequestration, is that the reservoir properties and trapping mechanisms are well known. Also, the oil and gas that originally accumulated in structural and stratigraphic traps did not escape for millions of years, demonstrating their integrity. The existing infrastructure can be utilized, or at least partially. However, there could be potential problems with reservoirs that have had a large number of wells, as these could act as leakage pathways for CO_2.

There can often be a large quantity of oil remaining in an abandoned oil reservoir. As such, it is very unlikely that it will be used as a storage facility unless some form of enhanced oil recovery is combined into the CO_2 storage system. This can be compared with an exhausted gas reservoir, where usually up to 90% of the original content would have been removed and the reservoir can be genuinely regarded as depleted and available for CO_2 storage (Global CCS Institute, 2019).

The total global storage potential of all oil and gas fields in the world is estimated to be 670 Gt of CO_2 (180 Gigatonnes of Carbon [GtC]) assuming the entire volume can be mobilized with CO_2 at some point in the future. The distribution between oil and gas is 150 Gt CO_2 (40 GtC) and 520 Gt CO_2 (140 GtC) respectively (Global CCS Institute, 2019).

In order to reduce impurities and other substances in the CO_2 stream, appropriate CO_2 purification and pressurization steps are needed. This is because impurities in the CO_2 can significantly reduce the amount which can be stored, increase capital costs and enhance corrosion. Some legal questions also need to be resolved concerning ownership of the residual hydrocarbons in the CO_2 filled reservoirs (Global CCS Institute, 2019).

2.2.3.2 Deep Saline Aquifers

It has been shown that carbon dioxide storage into low to high permeability deep aquifers in sedimentary basins is a technically feasible storage option. Carbon dioxide is an ideal candidate for aquifer storage because of its high solubility in water and its high density at the relatively high pressures which occur in deeper aquifers. Deep aquifers have the largest potential capacity for CO_2 storage (Global CCS Institute, 2019).

Large amounts of CO_2 can be trapped by the formation pressure in deep aquifers that contain water with a high salinity content. The determining factors are the integrity of the reservoir and the temperature and pressure in the reservoir. At depths greater than 800 m, pressure and temperature of CO_2 would be over the supercritical conditions, which is desirable from a storage perspective. World estimates of this storage option differ significantly due to different assumptions with respect to aquifer volumes, percent of the reservoir filled, density of CO_2 under reservoir conditions, and the volume suitable for storage. The storage capacity ranges from 87 GtC to 14,000 GtC if structural traps are not required for secure storage (Global CCS Institute, 2019).

2.2.3.3 Unminable Coal Beds

Due to the fact that CO_2 should not be stored in potentially minable coals, the percentage that could be used for CO_2 storage is relatively small. For pressures and temperatures above the CO_2 critical point, adsorption is gradually replaced by absorption and the CO_2 dissolves in coal. Carbon dioxide acts as a plasticizer for coal, diminishing the temperature required to cause a transition between a brittle, glassy structure, to a plastic and rubbery structure. This coal softening may adversely affect the permeability that would permit CO_2 injection. Similarly, coal swells when CO_2 is absorbed and/or adsorbed, reducing injectivity by orders of magnitude or more (Shi, Durucan & Korre, 2013, p. 37) but may be controlled by increasing the injection pressures (Larsen, 2004, p. 63-70). It is

very probable that if the coal is never exploited, the CO_2 will be stored for geological time, but any disturbance in the formation could void any storage (Metz, 2005, p. 217).

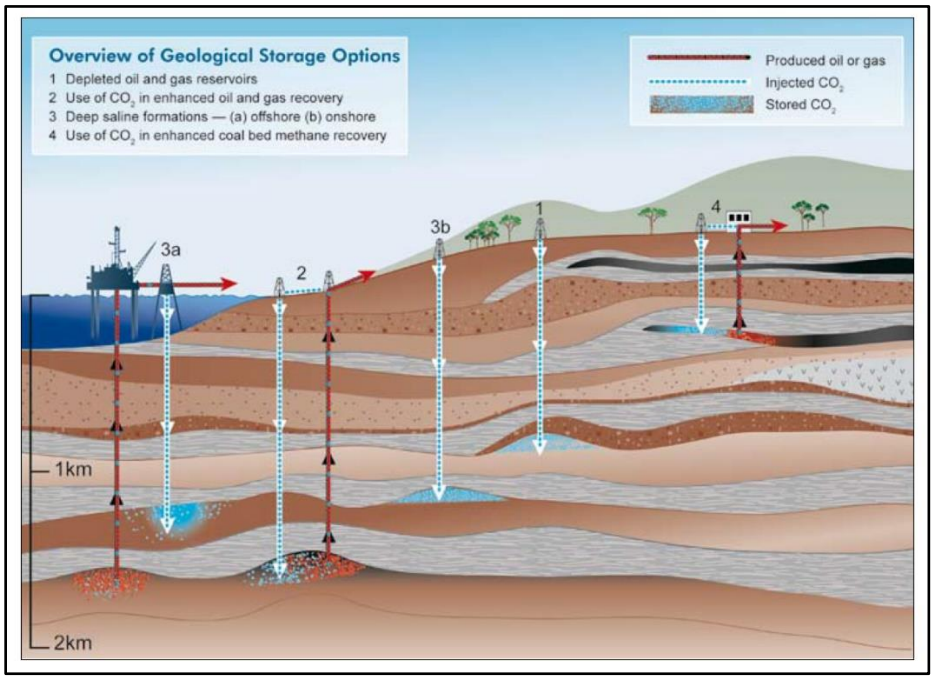

Figure 12. Types of Geological Formations for CO_2 Storage, modified from Metz, B. (2005). IPCC special report on carbon dioxide capture and storage. Cambridge: Published for the Intergovernmental Panel on Climate Change, Cambridge University Press

2.2.4 Trapping Mechanisms

As aforementioned, the overall effectiveness of geological storage depends on a combination of geochemical and physical trapping mechanisms. The most reliable storage sites are those where CO_2 is immobile because it is transformed into solid minerals or is adsorbed on the surface of coal micropores or it is permanently trapped under a thick, low permeability seal.

2.2.4.1 Structural/ Stratigraphic trapping

It is the most dominant of the trapping mechanisms and it shown in Figure 13. When injected, the supercritical CO_2 can be more buoyant than the other fluids present in the pore space. Therefore, the CO_2 will percolate up through the porous rocks until it reaches the top of the formation and this

is when CO_2 is trapped below low permeability rocks such as mudstone or shalestone, in order to avoid rapid migration of CO_2 to the surface. If the top of the trap is closed it could be expected for the CO_2 to remain in the trap for geological time periods (CO_2 Capture Project, 2019). Additionally, the production of oil and natural gas from sedimentary basins creates low pressure storage space that can be repressured with carbon dioxide. A careful characterization of the reservoir is necessary because buoyant CO_2 will seek out of the high permeability pathways, including fractures, faults, wellbores and interconnected aquifers (Global CCS Institute, 2019).

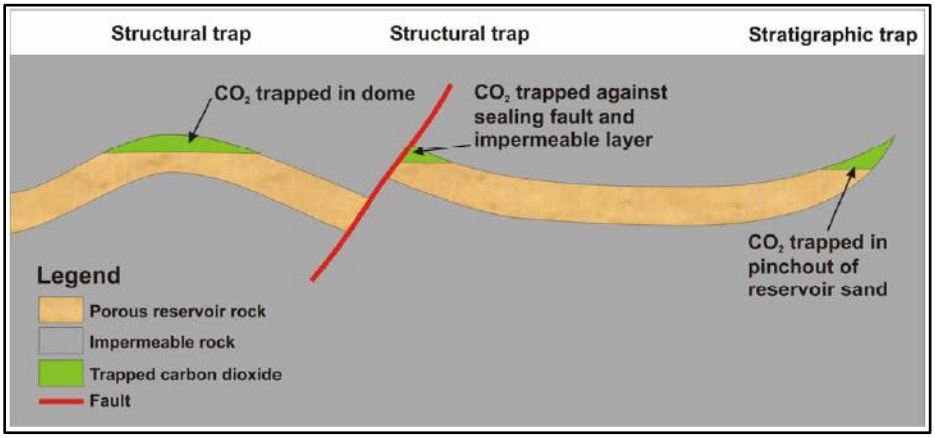

Figure 13. Structural Trapping, retrieved from https://hub.globalccsinstitute.com/publications/industrial-carbon-dioxide-emissions-and-carbon-dioxide-storage-potential-uk/52-co2-trapping-mechanisms-aquifers

2.2.4.2 Residual trapping

Residual trapping involves trapping carbon dioxide at the irreducible saturation point, segregating the CO_2 bubble into droplets that become trapped in individual or groups of pores. The porous rock acts like a rigid, tight sponge and as the supercritical CO_2 is injected into the formation it displaces fluids as it moves through the porous medium (Figure 14). As CO_2 continues to move, CO_2 again replaces it, but some part of the CO_2 will be left behind as residual droplets in the pore space, like water in a sponge (CO_2 Capture Project, 2019).

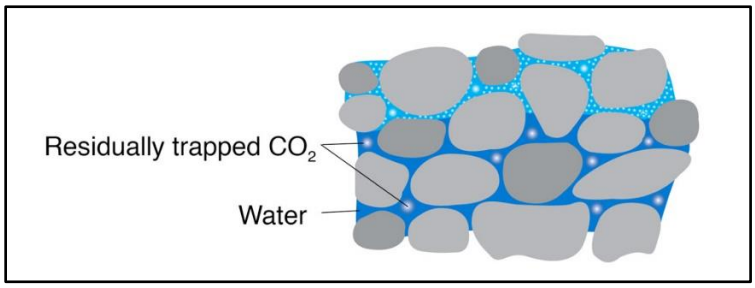

Figure 14. Residual Trapping, retrieved from http://www.dmp.wa.gov.au/FAQs-1478.aspx

2.2.4.3 Solubility trapping

When CO_2 is injected into deep saline aquifers (Figure 15), it can dissolve in the formation water on a time scale of decades (Law and Bachu, 1996, p. 1167-1174). Over longer periods of time, like century or millenia, all the injected CO_2 can dissolve if the structure allows it (McPherson & Cole, 2000, p. 84). Normally the amount of dissolved CO_2 decreases with depth as a result of increasing water salinity and temperature (Bachu & Adams, 2003, p. 3151-3175).

Carbon dioxide alters the pH as it dissolves in the aqueous phase. The following reactions take place:

Equation 9

$$H_2O + CO_2 \leftrightarrow H_2CO_3 \leftrightarrow HCO^-{}_3 + H^+$$

Some of the CO_2 is held as bicarbonate in the aqueous phase. No matter how high the pressure of the carbon dioxide, only minor amounts of the bicarbonate proton and ion will be produced. The proton is released when the CO_2 dissolves into the formation water, resulting in acid conditions for the water (Global CCS Institute, 2019).

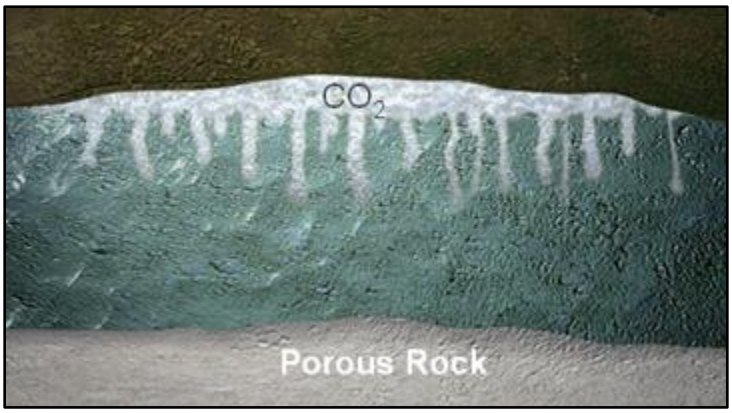

Figure 15. Solubility trapping, retrieved from https://www.co2captureproject.org/co2_trapping.html

2.2.4.4 Mineral trapping

By being acidic, the dissolved CO_2 can attract carbonate and silicate minerals (Figure 16) present in the aquifer as free ions of elements, like iron (Fe), magnesium (Mg) and calcium (Ca), while at the same time neutralizing the pH shift caused by the dissolved CO_2, allowing more bicarbonate ions to form. This is called ionic trapping, and one of the fastest precipitation reactions is that of calcium carbonate, this occurs when free calcium ions exist in supersaturated amounts in the presence of bicarbonate ions (Global CCS Institute, 2019). The reaction produces calcite, as shown below:

Equation 10

$$Ca^{2+} + HCO^{-}{}_3 \leftrightarrow CaCO_3 + H^+$$

The role of the silicate minerals in the above reaction is to neutralize the acid added to the formation water by the addition of CO_2. There are similar reactions for the formation of siderite (iron carbonate), dolomite (magnesium carbonate). The reactions that may occur in the aquifers are such that the CO_2 is permanently fixed as a mineral (Global CCS Institute, 2019). For more complex minerals commonly found in the aquifers, the reaction is of the form:

Equation 11

$$Feldspars + Clays + CO_2 = Kaolinite + Calcite + Dolomite + Quartz + Siderite$$

Where CO_2 is fixed permanently as carbonate minerals such as dolomite, siderite and calcite. Mineral trapping of carbon dioxide is favored in aquifers containing a large abundance of clay.

Figure 17 presents the contribution of the different trapping mechanisms through time.

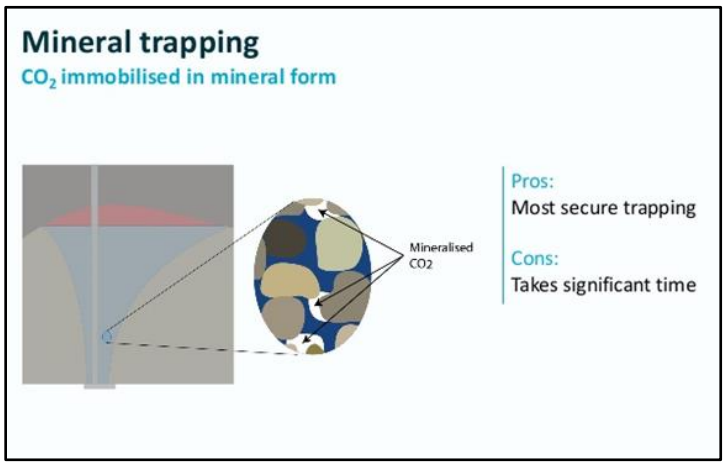

Figure 16. Mineral trapping retrieved from https://www.slideshare.net/globalccs/convective-mixing-in-geological-storage-of-co2

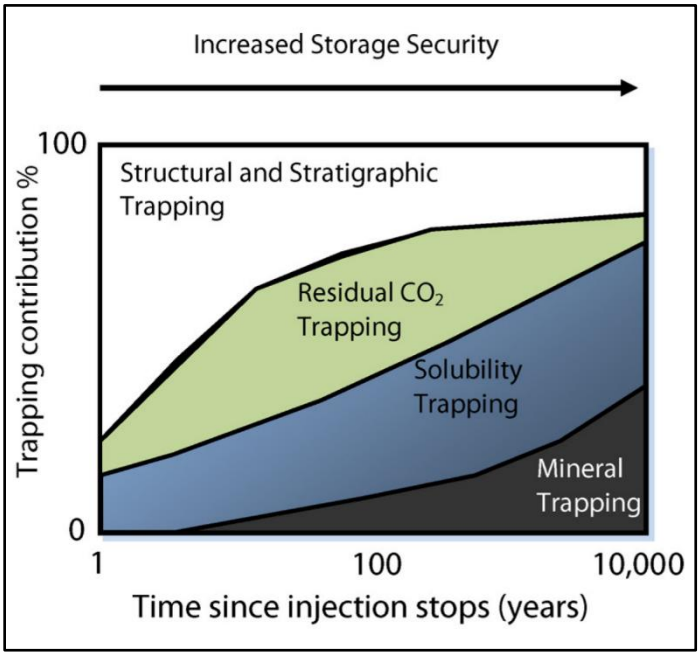

Figure 17. Trapping Mechanisms Contribution through time, retrieved from https://www.researchgate.net/figure/arious-mechanisms-for-trapping-of-CO2-From-1_fig5_248607869

2.2.5 Monitoring and verification

Monitoring for geological storage projects requires an overall risk management strategy. Essentially, injection well pressure and injection rate should be measured routinely. Repeated seismic surveys have shown to be useful for tracking the underground migration of CO_2. Novel techniques such as electrical and gravity measurements may also be advantageous (Metz, 2005, p. 35). For directly detecting CO_2 leakage the sampling of groundwater and the soil between the surface and water table could be beneficial. Surface-based techniques may also be used for detecting and quantifying surface releases and CO_2 sensors with alarms can be located at the injection wells for detecting leakages and ensuring worker safety. For spotting small rates of leakage, measurements will be crucial, this may be improved by high-quality baseline data that improve the reliability and resolution of information (Metz, 2005, p. 35). Based on observations and analysis of current CO_2 storage sites, the fraction retained in properly managed reservoirs is very likely to exceed 99% over a span of hundreds years, and it is possible to exceed 99% over 1000 years, as the risk of leakage is expected to decrease over time, while other mechanisms provide additional trapping, similar fractions retained are similar for even longer periods of time (Metz, 2005, p. 35). So, bearing in mind the former information stated, all of these monitoring techniques need to be tested and assessed in regard to sensitivity, resolution and reliability in the context of geological storage because they have been adapted from other applications and given the long-term nature of CO_2 storage, site monitoring may be required for very long periods (Metz, 2005, p. 34).

3.0 GEOLOGY OF THE SNØHVIT FIELD

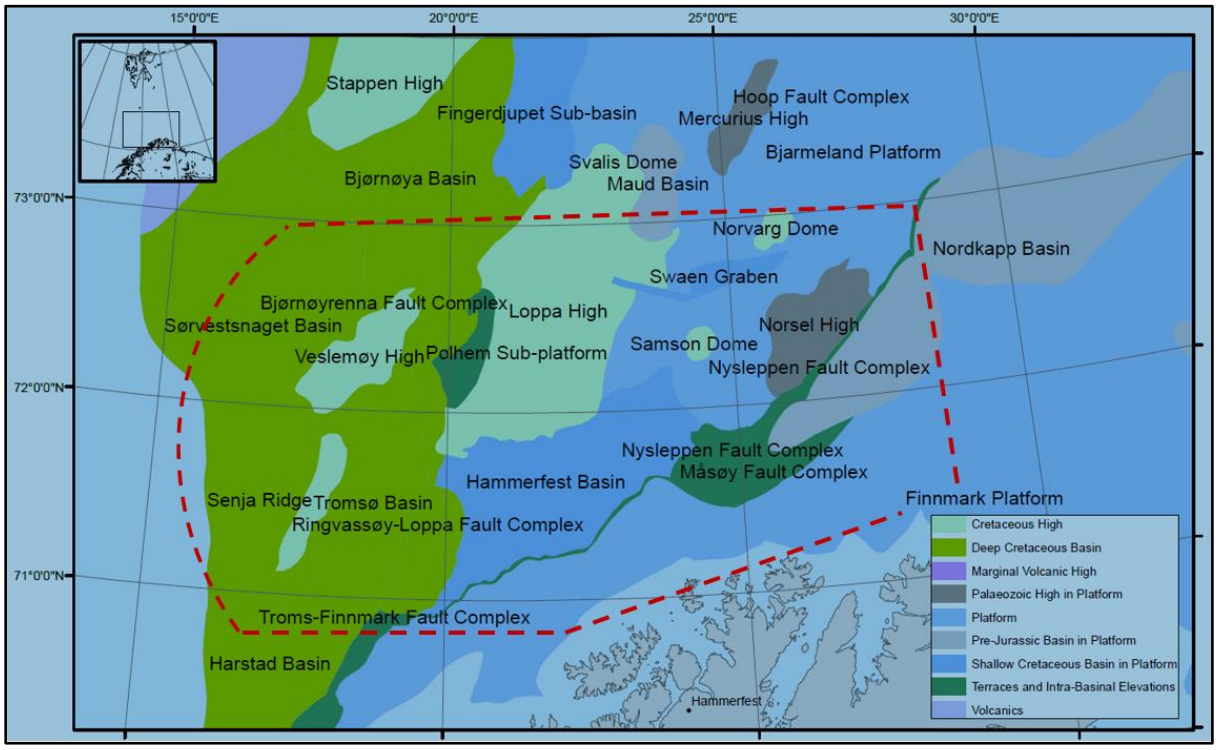

Figure 18. Structural elements of the Southern Barents Sea with a red dotted line showimg the zone evaluated for CO_2 storage (modified from Halland, E.K., Mujezinovic, J. and Riis, F. (Eds) (2014). CO_2 Storage Atlas: Norwegian Continental Shelf. Norwegian Petroleum Directorate, Stavanger.)

The Barents Sea is situated between Svalbard and the Norwegian continental shelf, and has been affected by several tectonic episodes after the end of the Caledonian orogeny which finished in the early Devonian and late Silurian (E.K. Halland, J. Mujezinovic and F. Riis, 2014, p. 25). The Snøhvit field is located in the Barents Sea at 71 degrees north, it was discovered in 1984 and it has a water depth between 310 and 340 meters (Norwegian Petroleum Directorate, 2018).

The southern part of the Barents Sea shelf is divided into various main structural elements. Amongst the most important found are the Bjarmeland and Finnmark Platforms, the Loppa High and the Hammerfest and Nordkapp Basins. Smaller structural elements also exist, like Veslemøy, Senja Ridge, Norsel High and the Polheim sub-platform. There is a number of fault elements that partially define and border the main structural elements, these are Bjørnøyrenna, Ringvassøy-Loppa, Masøy, Troms-Finnmark, Asteria and Nysleppen fault complexes (E.K. Halland et al, 2014, p. 25).

As shown on Figure 18, the zone evaluated by the Norwegian Petroleum Directorate for CO_2 storage was defined to the south/southeast by the Finmark Platform and the Troms-Finmark fault complex, to the east by a north-south line running around the 28 degrees meridian. To the west the area is defined by the Bjørnørenna and Ringvassøy-Loppa fault complexes trending from N-S to NNE-SSW and to the north it is defined by an east-west line approximately along the 73 degrees parallel (Halland et al, 2014, p. 25).

Snøhvit is located in an elongated east-west trending fault block system in the central part of the Hammerfest Basin (Kaufmann, R., Skurtveit, E., 2018, p. 10). This basin is fault controlled, to the south against the Troms-Finmark fault complex, to the north against the Asteria fault complex and the Bjarmeland platform, finally to the west controlled against the Ringvassøy-Loppa fault complex.

It is very possible that the basin was established by early to late carboniferous rifting. Major subsidence occurred in the Triassic, Jurassic and early Cretaceous overlain by a thin sequence of early Paleocene and late Cretaceous shale. Related to the late Jurassic tectonic episode, the basin is characterized by a faulted dome structure that has an internal central E-W trending (E.K. Halland et al, 2014, p. 25).

3.1 The Realgrunnen Group

Initially, the Realgrunnen Group was defined with its area in block 7121/5, in the west central Hammerfest basin. It is divided into four formations, the Tubåen, Stø, Nordmela and Fruholmen formations, as depicted in Figure 9. In the southern part of the Bjørnøyrenna fault complex, exploration wells have shown thicknesses of up to 871 m (Halland et al, 2014, p. 31).

The lithology in the lower parts is comprised by coals and shales while in the middle and upper parts it is comprised of pale grey sandstone. The lower Norian shales of the Fruholmen formation define the boundary below. Deltaic systems developed over the southern parts of the Hammerfest basin up through the Triassic, succeeding the transgression in the early Norian. Afterwards, in the early Jurassic, coastal marine environments were developed grading into a variety of tidal, shoreface and barrier environments from the Toarcian towards the Bajocian. The depositional

environments of the Realgrunnen subgroup consist of nearshore deltaic environments and are characterized by coastal and shallow marine reworking of fluviodeltaic and deltaic sediments (Halland et al, 2014, p. 31).

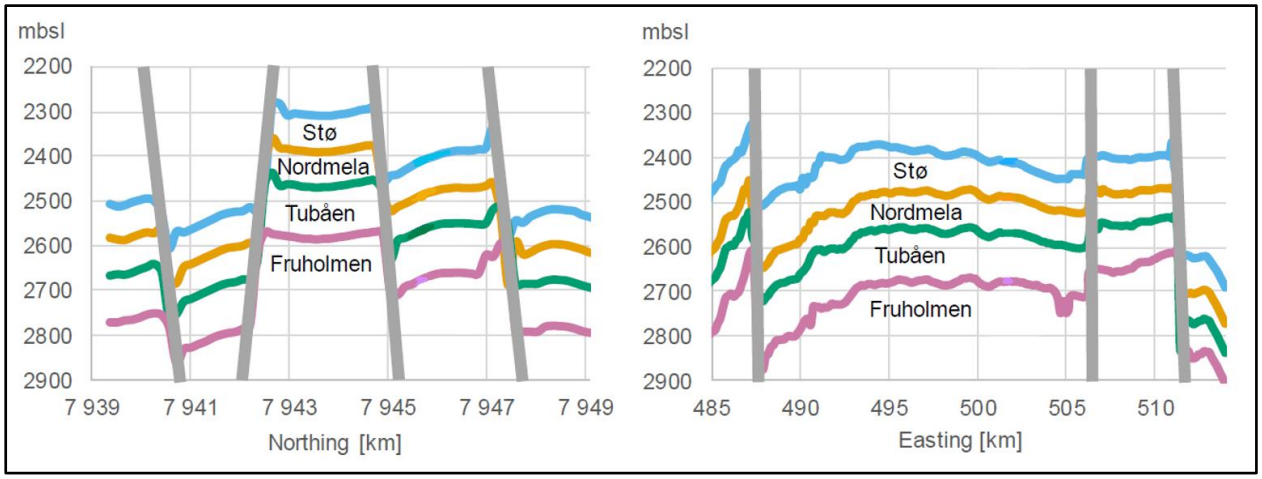

Figure 19. North-South and East-West cut plane Realgrunnen Group formations (modified from Kaufmann, R., Skurtveit, E. (Eds) (2018) "Snøhvit: A success story". FME SUCCESS publication)

3.1.1 The Stø Formation (Jurassic: Late Pliensbachien to Bajocian)

There are sandy sequences that form the Stø formation above the shale sediments of the Nordmela formation and phosphatic lag conglomerates can be found in the upper part of the Stø formation. The lithology of the Stø formation is well sorted mature sandstone. It is fairly noticeable that this formation thickens westwards in consistence with the underlying Nordmela formation. The last statement is evidenced by the thickness of 77m shown in type well (7121/5-1) and the thickness shown by the reference well (7119/12-2) with a value of 145m. Characteristics regarding thickness and depth are further exemplified in Figure 20. The unit may be subdivided into three depositional episodes with bases defined by transgressions. The uppermost (Bajocian) unit is highly variable due to syn-depositional uplift, and to later differential erosion. The middle part (Upper Toarcian-Aalean) represents the maximum transgression in the area and the basal unit is only present in the western parts of the Hammerfest basin (Halland et al, 2014, p. 35).

The sands in the Stø formation were formed in depositional environments known as prograding coastal regimes, a variety of linear clastic coast lithofacies are represented (Halland et al, 2014, p. 35).

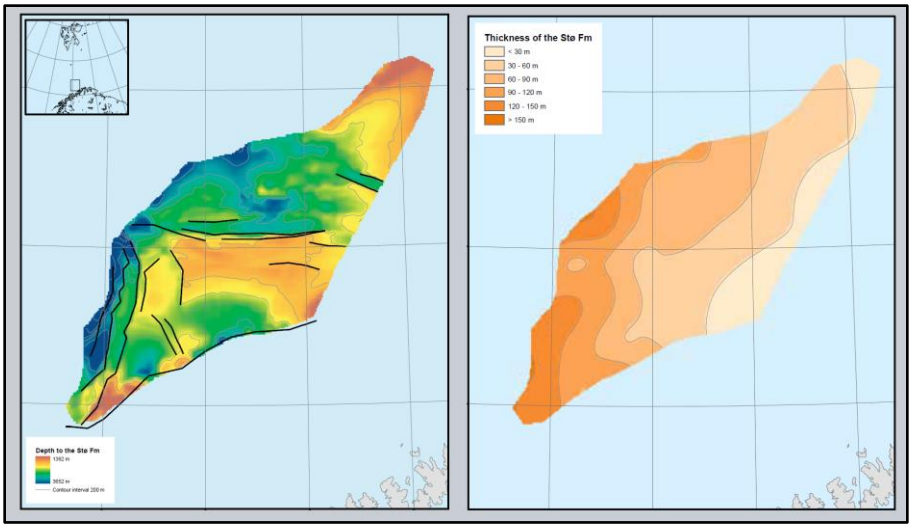

Figure 20. Depth and Thickness of the Stø Formation (Halland, E.K., Mujezinovic, J. and Riis, F. (Eds) (2014). CO_2 Storage Atlas: Norwegian Continental Shelf. Norwegian Petroleum Directorate, Stavanger.)

3.1.2 The Nordmela Formation (Jurassic: Sinemurian-Late Pliensbachian)

The lithology consists of interbedded sandstones with minor coals, shale and mudstones. Here the sandstones seem to be more developed towards the top of the structure.

In the reference well (7119/12-2) the depth is 202m and in the well (7121/5-1) the thickness is 62m. This illustrates a southwest thickening wedge in the Hammerfest Basin, similar to the underlying Tubåen formation. Westward thickening is characteristic for all the three Lower and Middle Jurassic formation and may be the result of early Kimmerian subsidence (Halland et al, 2014, p. 34).

Individual sandstones represent estuarine and tidal channels, moreover the formation represents deposits in a tidal flat to flood-plain environment (Halland et al, 2014, p. 34).

3.1.3 The Tubåen Formation (Triassic-Jurassic: Late Rhaetien to early Hettangian)

The lithology is dominated by sandstones with minor coals and shale. The formation can be largely divided into three parts, with an upper and a lower sand-rich unit separated by an interval comprised mostly by shales.

In this formation, the shale content increases towards the northwest that might generate interfingering with a lateral shale equivalent. Information regarding the thickness of the formation presented a maximum thickness of 261m from well 7120/6-1 in the Snøhvit field. The sandstones of the Tubåen formation are thought to represent stacked series of fluviodeltaic deposits. While marine shales reflect more distal environments to the northwest, though coals in the southeast were deposited in environments known as back barrier lagoonal (Halland et al, 2014, p. 33).

3.1.4 The Fruholmen Formation (Triassic: Norian to Rhaetian)

This lithological development consists of grey to dark shale passing upwards into interbedded shale, coals, and sandstone. The upper part is dominated by shales whilst the middle part of the formation is dominated by sands. This has therefore resulted in a threefold subdivision of the formation with shale rich Krabbe member at the top, overlying the sandier Reke Member and having the shale-dominated Akkar Member at the base. In the reference well (7129/9-2) the thickness of the formation is 262m and in the type well (7121/5-1) the thickness is of 221m (Halland et al, 2014, p. 32).

The depositional environment has been interpreted as open marine shales in the Akkar formation passing into fluvial and coastal dominated sandstones in the Reke formation. Representing northward fluviodeltaic progradation (Halland et al, 2014, p. 32).

3.2 Other Structures in the Hammerfest Basin

3.2.1 Albatross

Albatross is an underfilled structure, and presents a structural spillpoint direction towards the east. Apparently, due to the presence of deteriorated seismic signals to the west, there is evidence of a

significant gas related zone. Also, a fault intersection has been recognized above the gas-water contact in this field, where the northern east-west structure bounding faults intersects a minor fault orientated roughly north-south. Vertical leakage at this intersection explains the current position of the gas-water contact. The location of the chimney coincides with the intersection of faults which is exposed in more detail in figure 21 (Hermanrud, C., Halkjelsvik, M. E., Kristiansen, K., Bernal, A., & Strömbäck, A. C., 2014, p. 231).

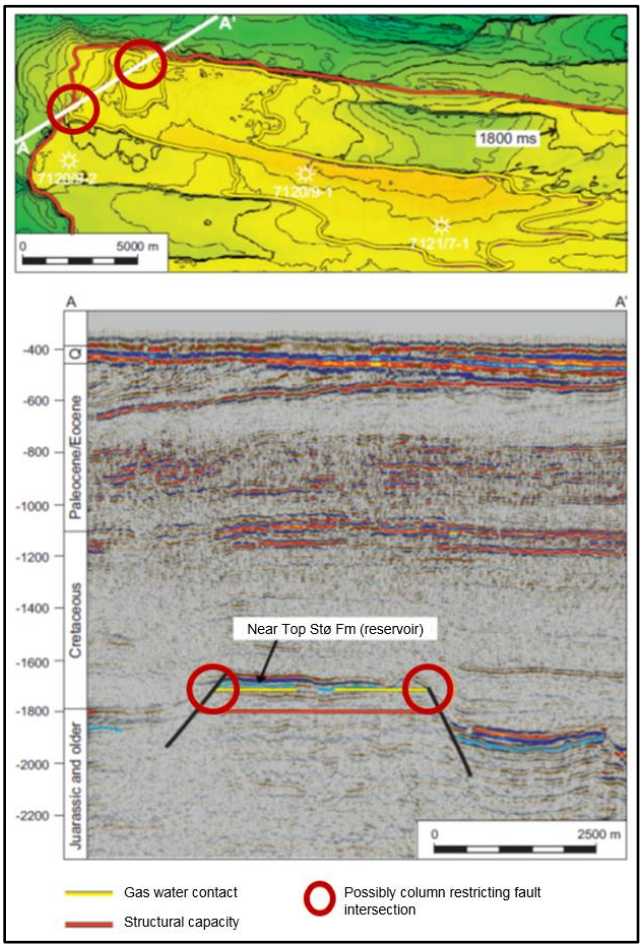

Figure 21. Albatross structure (modified from Hermanrud, C., Halkjelsvik, M. E., Kristiansen, K., Bernal, A., & Strömbäck, A. C. (2014). Petroleum column-height controls in the western Hammerfest Basin, Barents Sea. Petroleum Geoscience, 2014)

3.2.2 Snøhvit Nord

The structure has a dome shape and it is cross-cut by several second order faults. A fault intersection is present to the west, where it coincides with the position of the gas water contact. At

the southeast corner of the field the gas water contact gradually narrows off to zero, were once again it coincides with an intersection of an NE-SW and east to west striking faults. No other faults were identified above the gas water contact, as shown on Figure 22. The structure is similar to that of Albatross in that two fault intersections have been identified, both of which coincide with the position of the gas-water contact (Hermanrud, C. et al, 2014, p. 230).

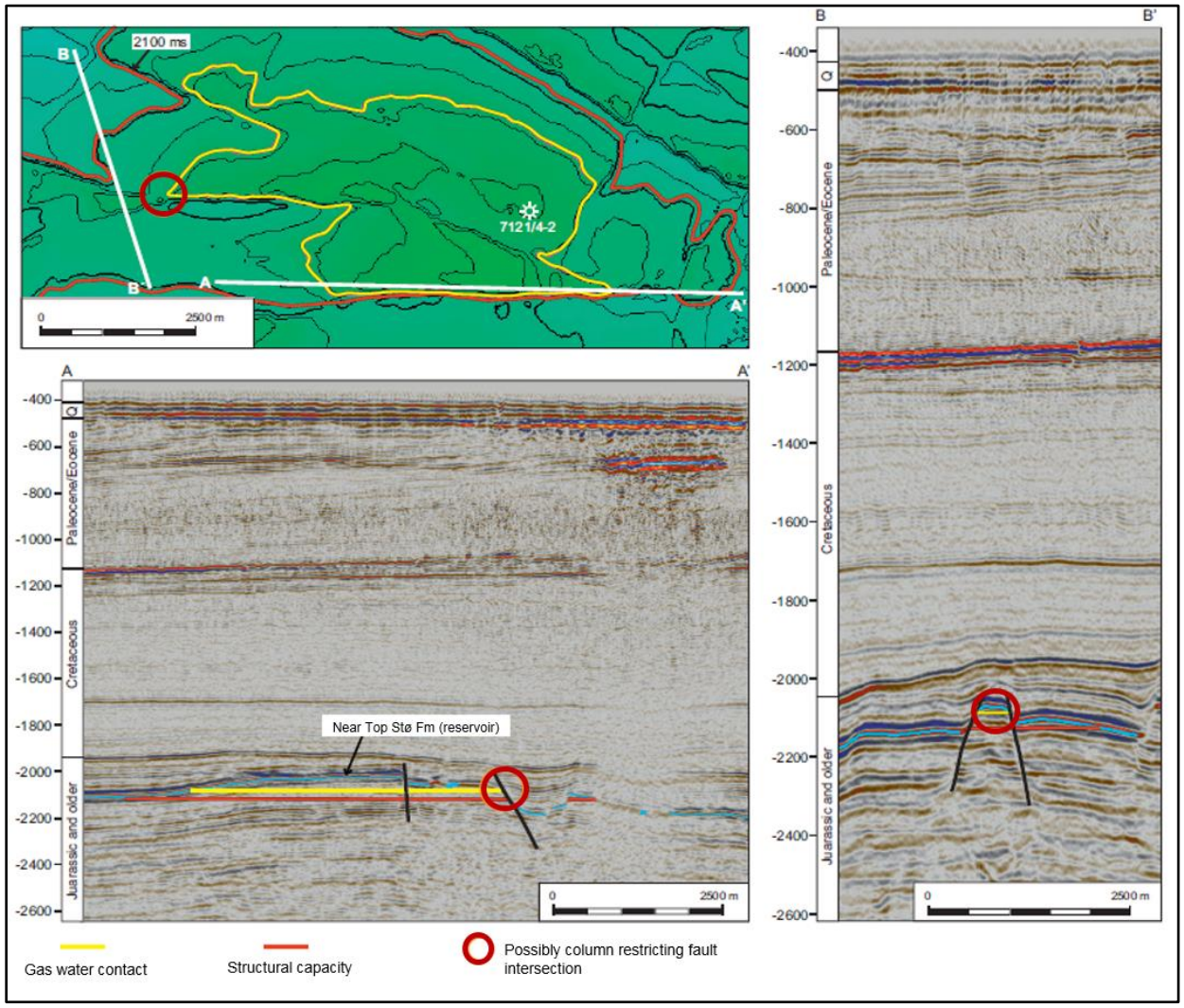

Figure 22. Snøhvit Nord structure (modified from Hermanrud, C., Halkjelsvik, M. E., Kristiansen, K., Bernal, A., & Strömbäck, A. C. (2014). Petroleum column-height controls in the western Hammerfest Basin, Barents Sea. Petroleum Geoscience, 2014)

3.2.3 Askeladden

The Askeladden structures are situated at terraces west of the north-south dome structure that dominates the eastern part of the Hammerfest Basin. These structures are called Askeladden Vest, Sør and Gamma.

The Askeladden Sør structure is not filled to its structural capacity and it is delineated by an east-west fault to the north (Figure 23). This fault intersects the north-south bounding fault at the apex of the structure close to 90, and has not emptied it. The only other notable fault intersection of this structure intersects the top of the reservoir surface where the fluid contact tends to be zero.

The Askeladden Vest structure is situated on the main terrace between the other Askeladden fields and the Tromsø Basin. It is the first large structure that received gas charge from the Trømso

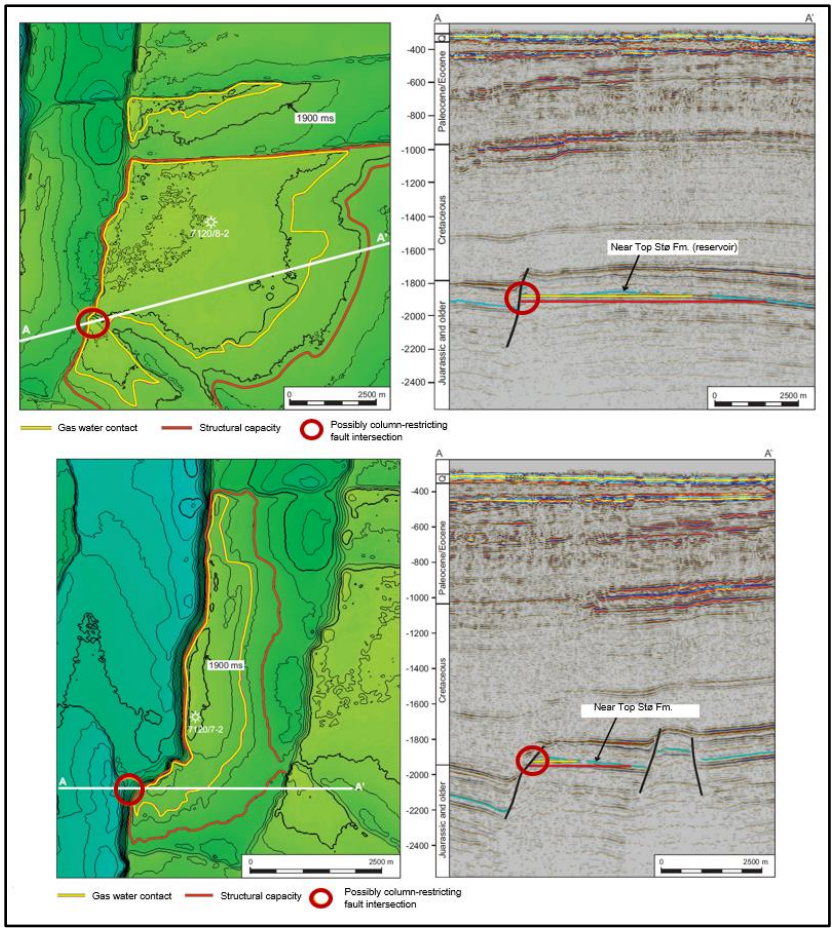

Figure 23. Askeladden a) Sør & b) Gamma structure (modified from Hermanrud, C., Halkjelsvik, M. E., Kristiansen, K., Bernal, A., & Strömbäck, A. C. (2014). Petroleum column-height controls in the western Hammerfest Basin, Barents Sea. Petroleum Geoscience, 2014)

Basin, and it spilled towards Askeladden Gamma at the time of maximum filling. At its western flank, the structure is defined by an array of interlinked north-south faults. The northernmost of these faults do not displace the Upper Cretaceous and younger strata, signifying that the later tectonic events along the Ringvassøy-Loppa fault complex were taken up by faults further to the west. The southernmost north-south faults do in fact, displace strata. The intersection of these interlinked north-south trending faults takes place at the the top of the reservoir surface, above the present-day gas-water contact. On the other hand, the gas-water contact coincides with an intersection between an east-west and NW-SE fault at the NE part of the structure (Hermanrud, C. et al, 2014, p. 232-234).

When the Askeladden Gamma structure was filled to its spillpoint, it is interpreted to have spilled to the southern part of Askeladden Sør. The structure is located on a terrace just west of Askeladden Vest. The main north-south fault is a first order fault that offsets the Upper Cretaceous strata and this fault is intersected by three second-order faults striking approximately east-west. The northernmost fault appears to coincide with the location where the gas column tapers off to zero (Hermanrud, C. et al, 2014, p. 232-234). The Askeladden Vest structure is presented in Figure 24.

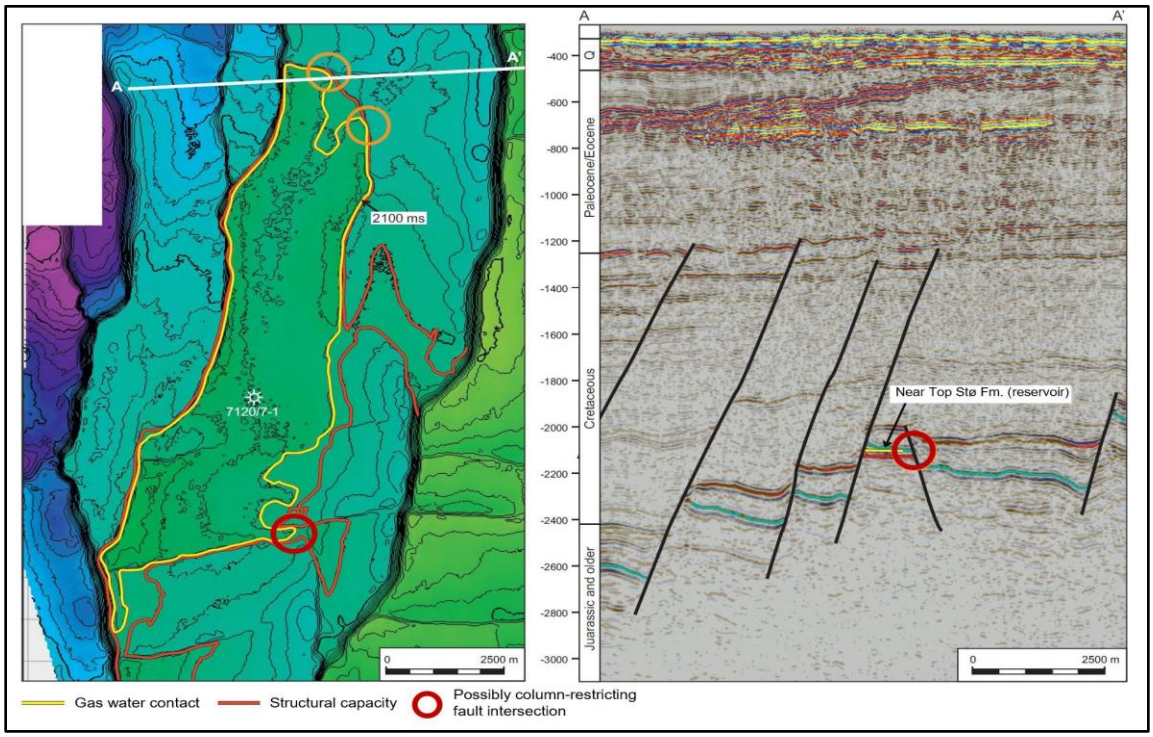

Figure 24. Askeladden Vest structure (modified from Hermanrud, C., Halkjelsvik, M. E., Kristiansen, K., Bernal, A., & Strömbäck, A. C. (2014). Petroleum column-height controls in the western Hammerfest Basin, Barents Sea. Petroleum Geoscience, 2014)

3.3 Storage Options: Saline Aquifers in Snøhvit

CO_2 associated with the production of natural gas in the Snøhvit field is separated at Melkøya and injected into the aquifer of the field. In sites where the pressure is high enough to surpass the minimum miscibility pressure (MMP) of oil and carbon dioxide, CO_2 injection may be considered as a means for tertiary recovery (CCUS) (Halland et al, 2014, p. 42).

The Hammerfest Basin aquifer consists of Lower and Middle Jurassic sandstones that are a part of the Realgrunnen subgroup, its area is represented in Figure 25 by a yellow outline. The aquifer is bounded by the Ringvassøy-Loppa and Troms-Finmark fault complexes in the west and south, and by the Asterias Fault complex towards the Loppa High. It is classified as a half open aquifer, comprising the Tubåen, Stø and Nordmela formations, and there is an equilibrium in the pore pressure for the three formations. Salinities in the aquifer generally exceed 100000 ppm, making the formation water strongly saline. At standard conditions the water density in Snøhvit is around 1.1 g/cm3.

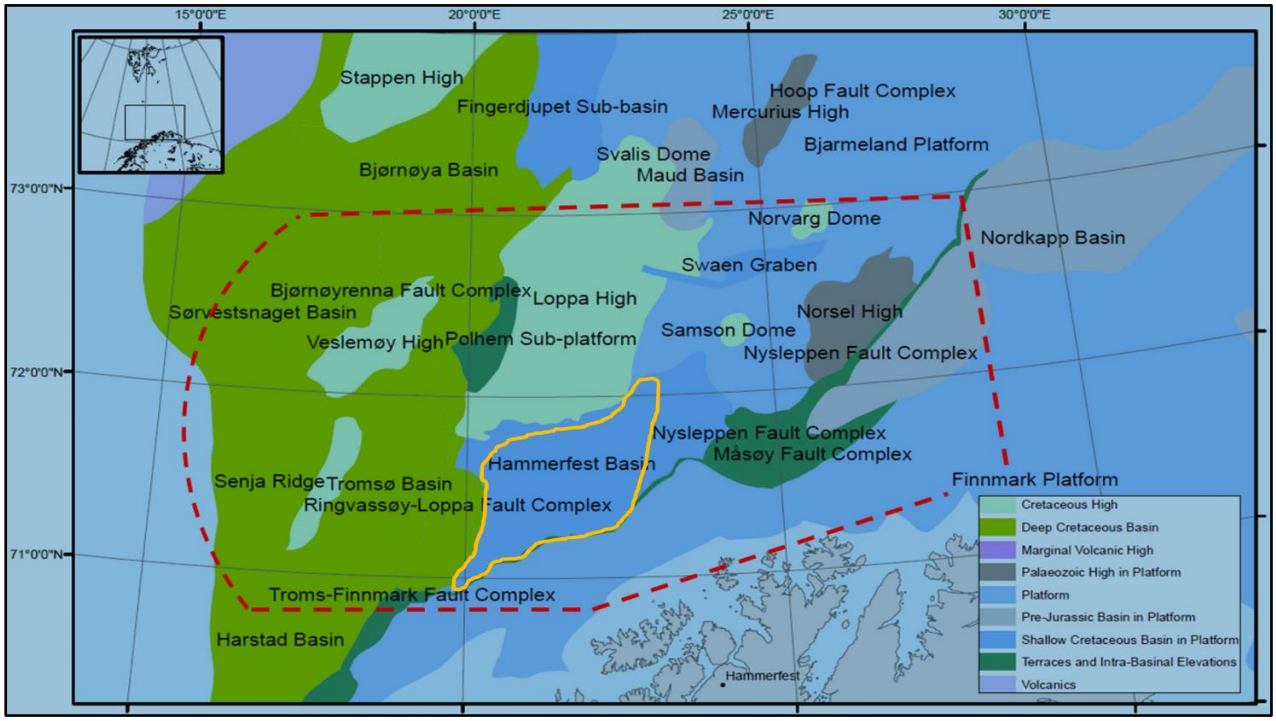

Figure 25. The evaluated area (red dotted) and the Hammerfest Basin Aquifer (orange outline) (modified from Halland, E.K., Mujezinovic, J. and Riis, F. (Eds) (2014). CO_2 Storage Atlas: Norwegian Continental Shelf. Norwegian Petroleum Directorate, Stavanger.)

This high salinity may cause problems for the storage because CO_2 is less soluble in brines than in sea water, the percentage of CO_2 trapped by dissolution can therefore be relatively small. Without mentioning the problems related to injection due to salt precipitation near the wells (Halland et al, 2014, p. 47).

Geological information has shown that the Stø formation is very well connected laterally. The experience from CO_2 injection in the Snøhvit field showed that CO_2 was contained within the Tubåen formation with no upwards migration into the Nordmela and Stø formations. In figure 26 the permeability is shown for the latter formations mentioned. This property has a higher range of values in the Stø formation and a lowest range of values in the Nordmela formation (Halland et al, 2014, p. 50).

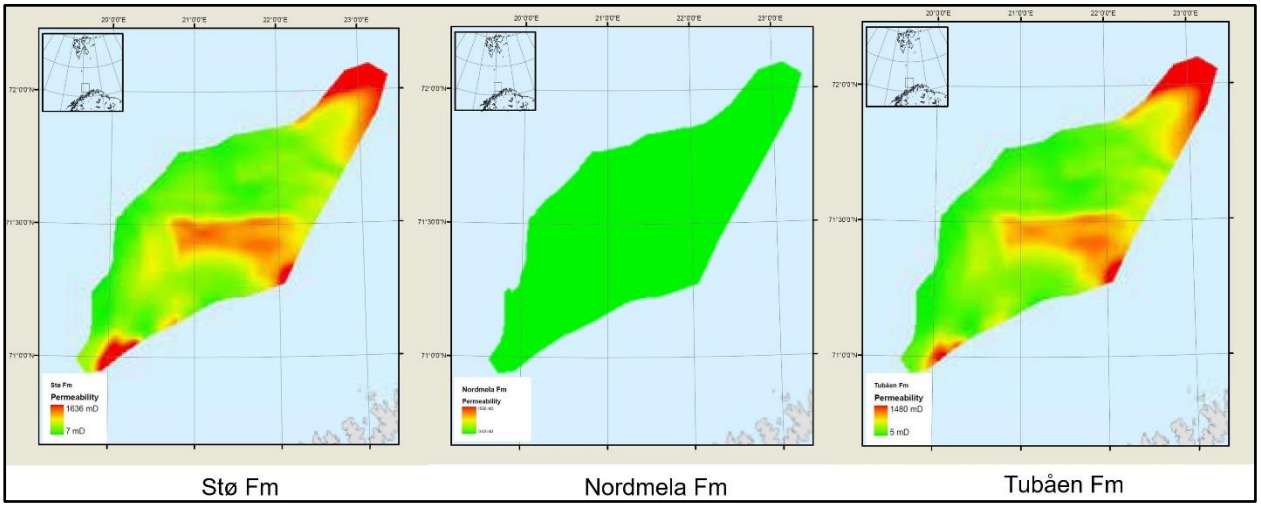

Figure 26. Permeability ranges in the Hammerfest Basin Aquifer (modified from Halland, E.K., Mujezinovic, J. and Riis, F. (Eds) (2014). CO_2 Storage Atlas: Norwegian Continental Shelf. Norwegian Petroleum Directorate, Stavanger.)

The calculations of storage capacity in the structures are based on injection and storage in the Stø formation. For the aquifer volume the storage capacity includes the Nordmela and Tubåen formations. The maximum and minimum pore volumes resulted in 6400 Mm^3 (Million cubic meters) and 680 Mm^3 respectively, for the Snøhvit Central Stø. These pore volume values indicate that there are sufficient aquifer volumes available to support the plumed CO_2 injection in the Stø formation (Halland et al, 2014, p. 51).

4.0 METHODOLOGY: THE SIMULATION MODEL

4.1 The Fluid Model

At first, the model was established by searching for information related to the composition of the fluids present in the reservoir. Several geochemical reports from the Norwegian Petroleum Directorate (NPD) Fact Pages were analyzed and there was one of particular interest that came from well 7121-4.2. The drilling depth was 2516 meters, the temperature was of 63 ºC and the pressure had a value of 27605 KPa (276.05 bar). Information regarding the composition of this sample is presented in Figure 27. At the depth mentioned, the fluid sampled was in gas phase. On the other hand, when pressure is lowered to surface conditions, there is presence of condensate.

Depth (m)	P (kPa)	T(°C)
2516 RKB	27605	63,6

SAMPLE	#2
Composition	
Gas	%
C1	88,36
C2	3,99
C3	1,46
i-C4	0,2
n-C4	0,39
i-C5	0,23
n-C5	0,22
C6	0,29
C7	0,2
C8	0,5
C9	0,32
C10+	0,48
CO2	2,71
N2	0,65

Figure 27. Composition from Sample 2 of well 7121-4.2.

Then this information was taken to Simulation Launcher, more exactly to PVTi, were by entering each percentage of the composition, the pressure, temperature and depth, a regression was completed like shown in Figure 28. In this point, the saturation pressure and the density of the liquid is regressed to show as low as possible percentage of error. The saturation pressure and the liquid density had errors of 0.13% and 3.27% respectively, which are low enough for the later

purposes. Afterwards it was possible to visualize the generated phase envelope like the one seen in Figure 29. In this figure, it is highlighted the zone where the sample of interest is located, the fluid behaving within the two-phase region. The main geological model for the Snøhvit field was provided by the Norwegian Petroleum Directorate (NPD). The fluid model for the latter particular case was compared to the one presented in PVTi, they rendered an acceptable match. Next, this fluid model was to be exported to Eclipse 300 which was the first option for running the model. However, when the segment model was to be opened in Eclipse 300, there was a high amount of errors and bugs that did not allow for it to be properly managed. Thus, in hopes of practicality, the decision for running the model in Petrel 2018 was taken.

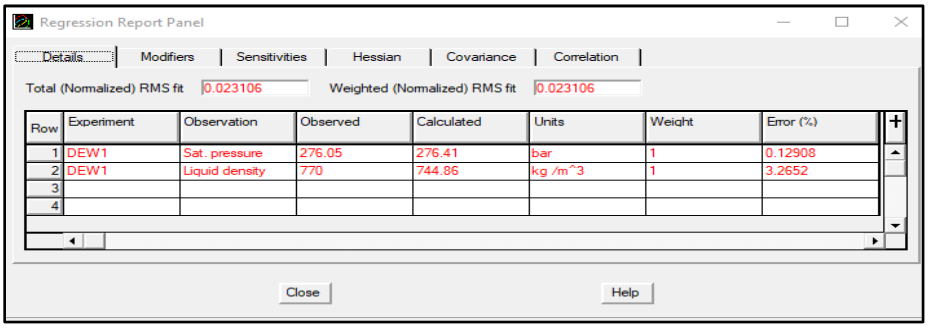

Figure 28. Regression Report Panel PVTi

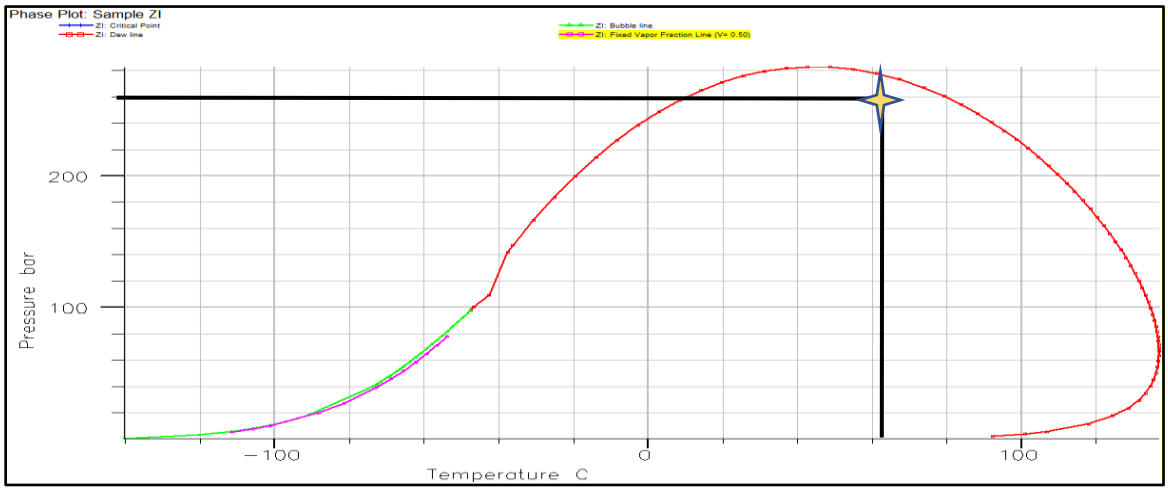

Figure 29. Fluid Sample Phase Envelope Well 7121-4.2

As shown, Figure 30 demonstrates that the saturation of gas in Snøhvit is quite high as it is a gas reservoir, more specifically a gas condensate reservoir. It can be seen how the saturation for the

different fluids is defined, gas saturation in red, oil saturation in green and water saturation in blue. The oil saturation, is supported by Figure 31 as well. There is evidence of hydrocarbon present as an oil phase but somewhat dispersed.

In Figure 31 the saturation of oil is colored from purple to blue, then to green, changing to yellow, passing to orange and finally to red, highlighting the saturation percentage of this zone. Being purple the value of 10% oil saturation and red the value of 90% oil saturation. According to the color difference that lie amongst light blue, green but mostly yellow and orange, it can be stated that the values for this property range between 45% and 85% in the main model.

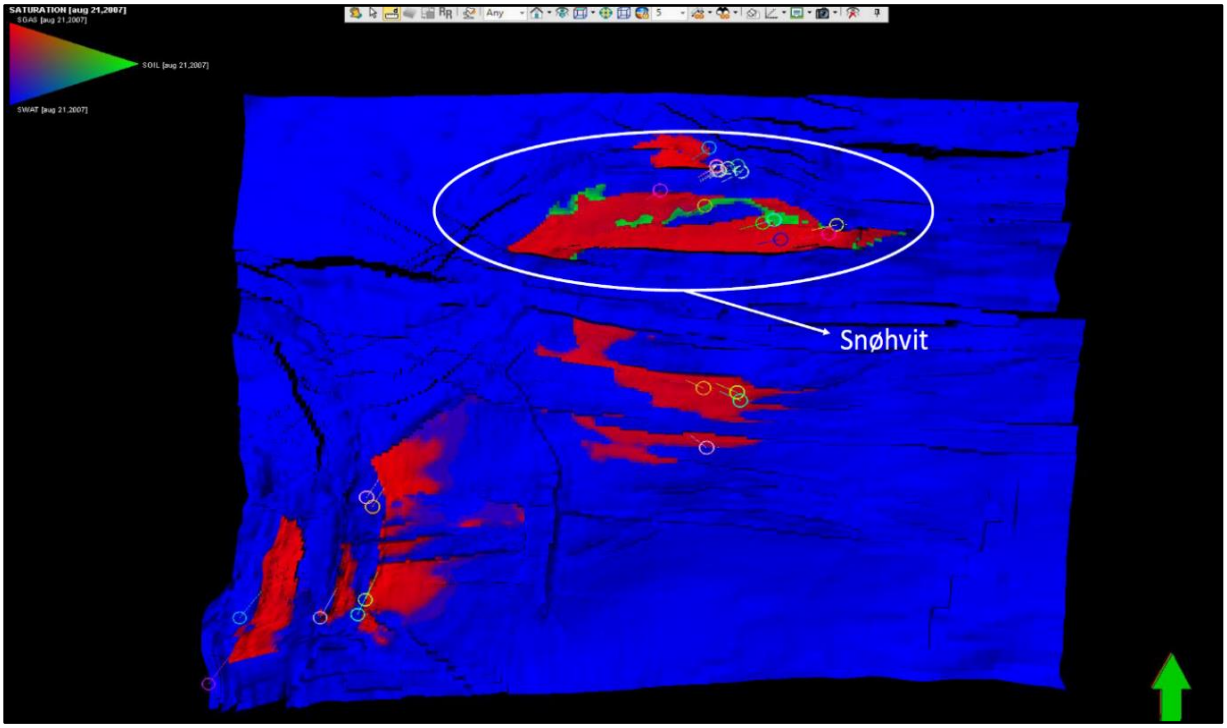

Figure 30. Saturation Variation (Gas, Oil and Water) Main Snøhvit field model

An arrow from East to West is shown in white color, as a reference to highlight the hypothetical path for the plume migration of CO_2 in the Stø formation, which is towards the west, in essence due to the direction of the fault block system and the development of several geological events.

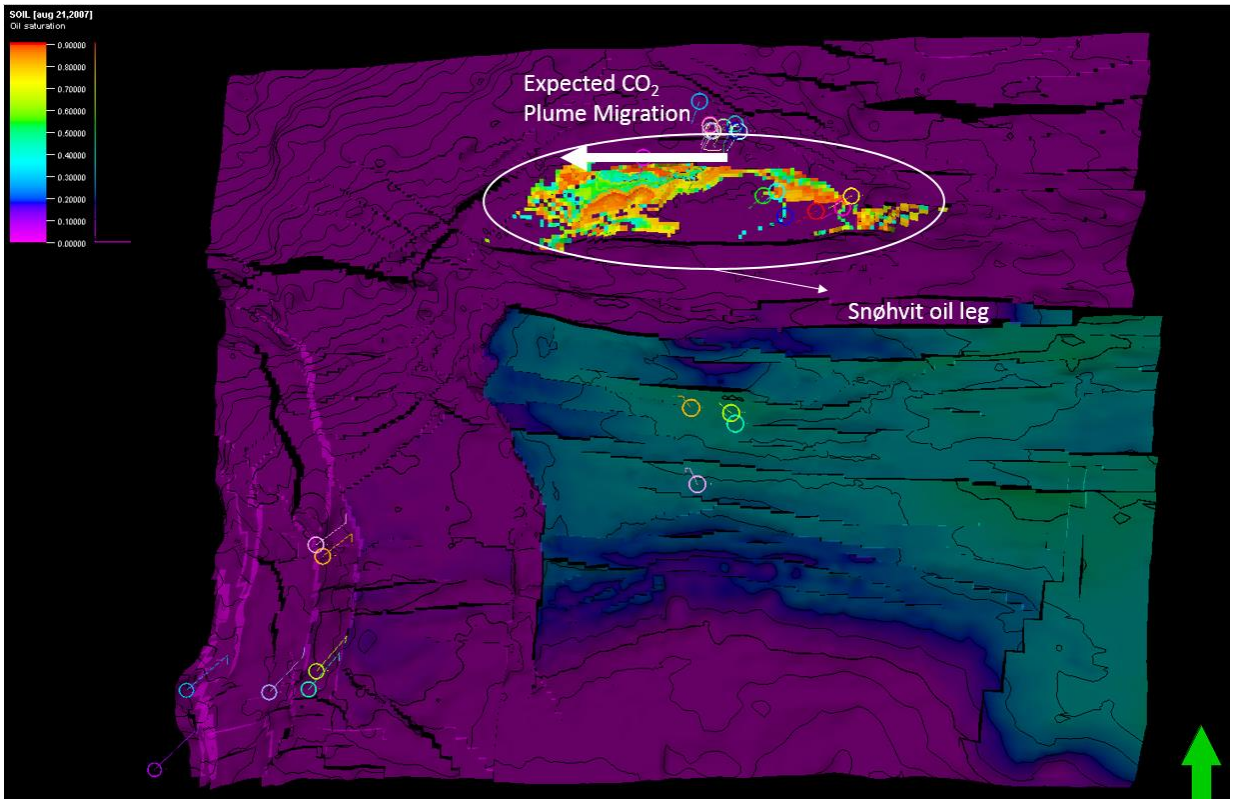

Figure 31. Oil Saturation in Snøhvit

The water saturation can be further presented in Figure 32, here it is clearly seen the Snøhvit gas field and the aquifer around and composing the Stø, Nordmela and Tubåen formations. Around 800.000 Sm^3/day of supercritical CO_2 are injected in Snøhvit and this is taken as reference for the Segment Model which will be explained further ahead. In Figure 32 it is also highlighted the area of the main field that is of further interest. It is important to note that the segment was taken in an area where there are no major faults present. The water saturation ranges from red color meaning zero percent and blue being 100% for water saturation. This will enable to view how is the behavior of the fluid injected in a zone where there is probability of encountering residual oil as gas condensate. This residual oil phase in Snøhvit has approximately 82.9 MRm^3 of oil which could be produced due to the action of the CO_2 being displaced close to this area of interest throughout time.

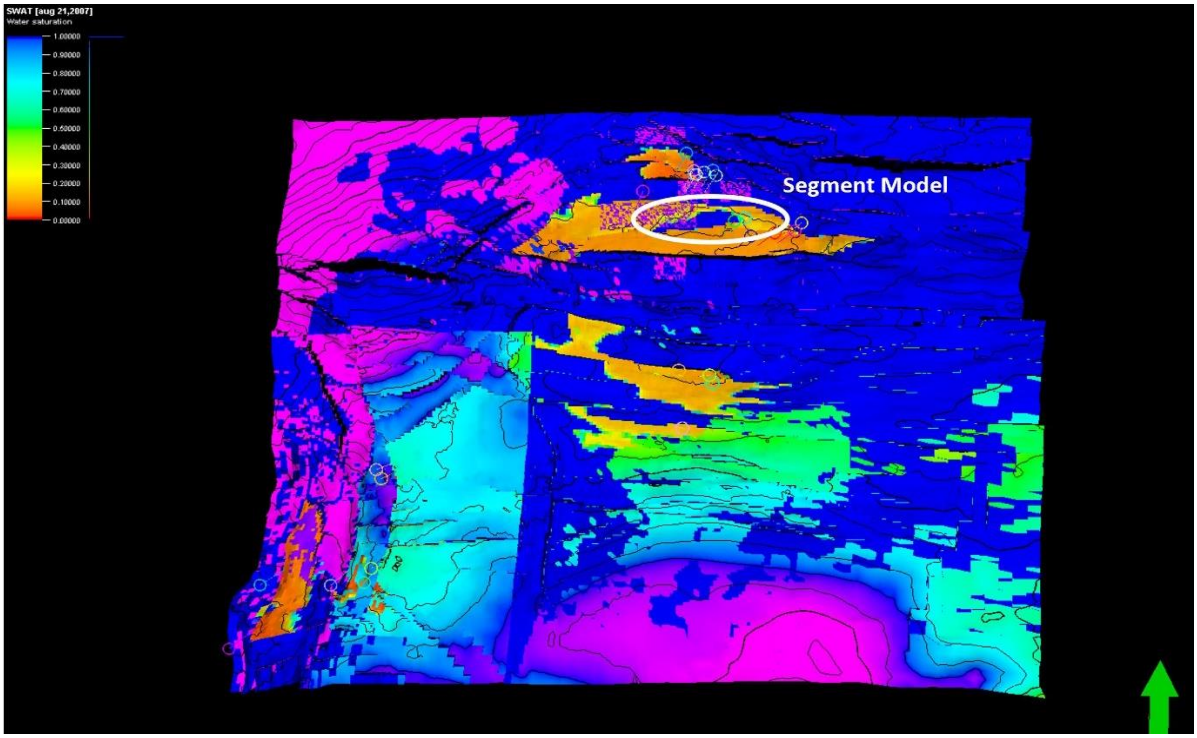

Figure 32. Saturation of Water in Snøhvit

4.2 Defining the Study Area

A polygon was created to show the most representative model as possible in order to understand the phenomena in question. For that reason, it was taken into account an area where the behavior of the CO_2 plume could contact a zone with a fair quantity of hydrocarbon. In Figure 33a it is possible to visualize the segment model with an upper view while Figure 33b and Figure 33c show a northwest to southeast view and a southwest to northeast view respectively. In the three images mentioned beforehand the CO_2 injector well is represented, as well as the producer well. Since the Figure 33 is shown in a far distance to be able to fully visualize the segment from different perspectives, the wells are represented as lines that connect to the model but they are not completely clear, nonetheless on the image, the injector well is emphasized as a green star and the producer well as a red diamond.

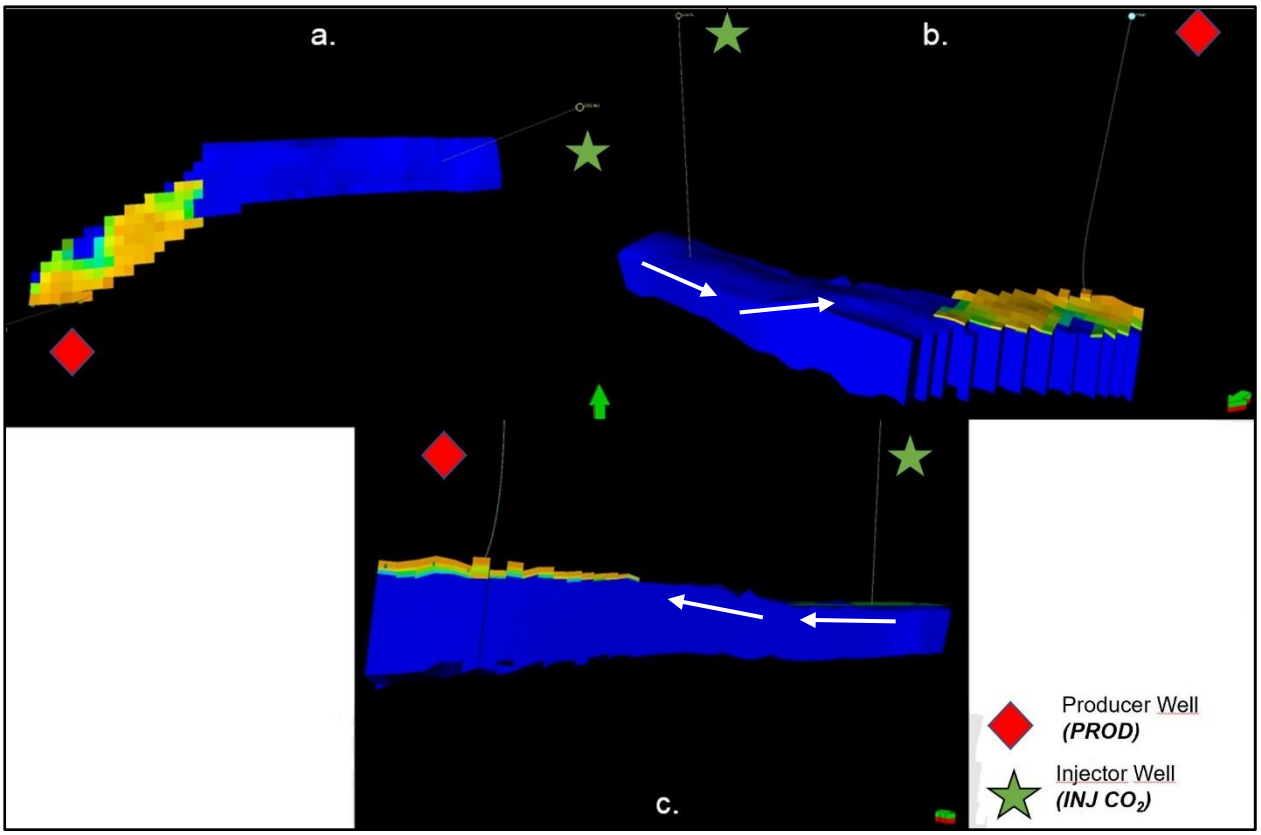

Figure 33. a) Upper View Segment Model, b) Northwest to Southeast View, c) Southwest to Northeast View

According to Petrel 2018, the segment model has 13567 meters of length. The value near the injector is of 1240 meters wide and close to the producer it is 1638 meters wide. Other values indicate that depths close to the injector are of 412 meters, while the depth close to the producer is of 522 meters. The distance between wells is 10059 meters. The figures show saturation with respect to water, making the region where the injector is located a part of the water zone (blue indicating 100% water saturation) where CO_2 storage began in 2011. As it will be mentioned in the next section, the development strategy for the segment model has been fixed to start January 1st 2011, since this is the year in which CO_2 started to be injected in the Stø formation. The producer well is located in a zone where there is petrophysical properties evidence of hydrocarbon being present. Although CO_2 sequestration began in Snøhvit as far back as 2008, but in a deeper formation, the Tubåen formation. After a while the pressure built up faster than was expected and an intervention was necessary in order to avoid fracturing the seal. In contrast to the deeper Tubåen formation, the Stø formation is in pressure communication with the gas producers on Snøhvit and no significant pressure buildup is expected in the injection location.

In Figure 33 it is possible to visualize the slope in the model, which is depicted more clearly by the arrows, this sort of difference in elevation is because the producer well is placed on a higher zone and the injector well is placed on the lower parts of the segment. This can have certain gravitational effects which may allow for the carbon dioxide to flow easier to the formations further above and in a way aid in the displacement of the hydrocarbon towards the perforations of the producer well. There are several factors and variables to be aware of during the calculation made by the software:

- Bottomhole pressure from the producer ***(PROD)***
- Production control rate ***(PROD)***
- Bottomhole pressure from the injector ***(INJ CO_2)***
- Perforation length from the producer ***(PROD)***

4.2.1. The Injector Well

The injector well was named ***CO_2 INJ*** and it is important to note that in reality the CO_2 injector already exists. It is located at a subsea true vertical depth (SSTVD) of 2526m and has perforations of about 120 m. The schematic of the ***CO_2 INJ*** is shown in Figure 34, and here it can be seen on the top right-hand side a scale of porosity where the conditions shown in blue where the most promising to perforate that area of the formation. In this part, the injection pressure has been established to 500 bar, if it is recalled from Figure 29 the fluid conditions are inside the envelope and because of the gas condensate reservoir conditions it is more advisable to keep the injection pressure high hence it is inside the envelope where the condensation of the heavier and intermediate fractions of the mix takes place. They are kept entrapped in the form of liquid in the smallest pores of the rock. Sometimes the critical saturation of the liquid is not reached and as consequence it cannot flow towards the wells. This circumstance represents a great aggravation for the production, owing to the fact that the part of major importance in the reservoir is the trapped liquid, rich in heavy components, but in exchange in certain situations, a much poorer fluid made up from these components is produced.

Notwithstanding, several runs were made in Petrel 2018, in order to find the best parameters for the means of better understanding the behavior of the CO_2 plume when moving towards the hydrocarbon. In a particular run, the injection rate of the ***CO_2 INJ*** was lowered down to 200.000

Sm^3/day and the results showed that the oil cumulative production was of 80.000 Sm^3. The cumulative water and gas production were 16 MSm^3 (Million standard cubic meters) and 5100 MSm^3 respectively. All the former in the span of 34 years of tertiary recovery operations in the segment model.

Another condition was set for injecting 400.000 Sm^3/day and this showed a slight increase to 94.000 Sm^3 of the cumulative oil production. The water cumulative production presented a value of 29 MSm^3 and the gas cumulative production had a value of 6000 MSm^3, which appeared to also show an increase.

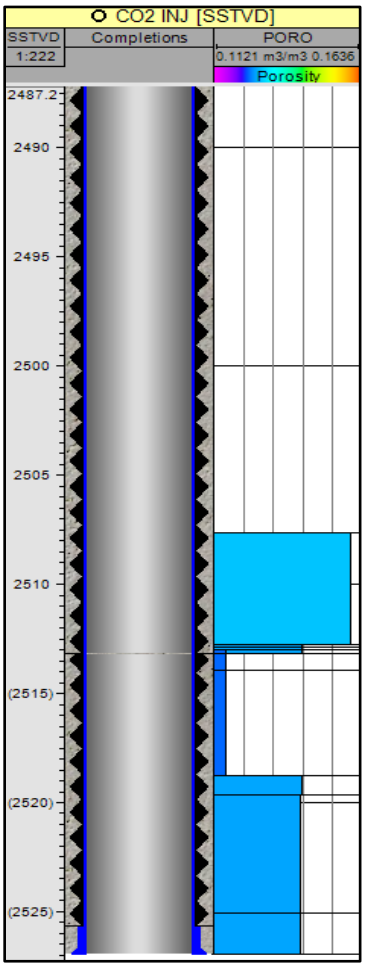

Figure 34. CO_2 INJ Well depth and porosities

4.2.2. The Producer Well

The producer well was named ***PROD*** but this particular well in reality does not exist. In Petrel 2018, it is located at a subsea true vertical depth (SSTVD) of approximately 2408 meters and has perforations of about 500 meters in order to make it easier to produce the hydrocarbon from the Stø formation. The schematic of the ***PROD*** is shown in Figure 35 and here can be seen the scale of porosity at the right side, where the conditions shown in blue where the most promising to perforate that area of the formation as well. In an earlier run the value for the perforations for the horizontal well was of 50 meters, and the oil rate equivalent per day rendered very little results having a rate of 0.2 to 0.4 Sm^3/day from an early time in the prediction setup. Besides that, the pressure development around the producer was quite high, having an average value of 2000 bar throughout time. This was a really high-pressure average for the reservoir, which would undoubtedly fracture the rock, so the fluid simulated just got dispersed rather than being produced.

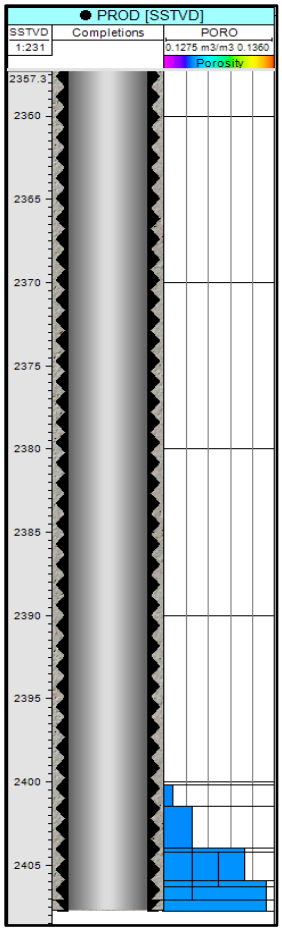

Figure 35. PROD Well depth and porosities

Thus, in another case study, the perforation lengths were increased to 500 meters, and conditions in the producer were fixed to have a bottomhole pressure of 150 bars, the bottomhole pressure for the injector well was lowered to 300 bars. The case rendered results that increased the cumulative oil production to 110.000 Sm^3, showing an increase of around 20.000 Sm^3 of oil. The cumulative water production was of 20 MSm^3, and the cumulative gas production evidenced to be quite similar to an earlier run, having a value of 5200 MSm^3.

On the other hand, the pressure average behavior had a lowest value of 168 bars in 2013, but then increased to around 180 bars and was maintain in a range that did not go above 190 bars for the entire prediction run. The choice for the placement of the wells is in general terms to take advantage of the geological formation at which the carbon dioxide is injected to make it easier for it to flow towards the zone where the hydrocarbon phase exists.

The well pressure production control conditions set in most of the cases was of 100 Sm^3/day, including the cases discussed above, but it was found that by reducing this number, the water production was delayed in approximately 3 years. These findings will be discussed in the next chapter.

For the matter discussed above the model has been set with the following operating restrictions:

Table 1. Rates, Pressure Controls and Perforations Lengths in the Producer Well (PROD)

Oil Production Rate	50	Sm^3/day
Bottomhole Pressure	50	bar
Perforation Length	500	meters

Table 2. Rates and Pressure Controls in the Injector Well (CO_2 INJ)

CO_2 Injection Rate	800.000	Sm^3/day
Bottomhole Pressure	500	bar

4.3 Development of the Field Management Strategy Prediction

The segment model was given certain conditions ran from Development Strategy option in Petrel 2018 starting at the date of January 1st 2011 until January 1st 2045. Overall setting the prediction time for a total of 34 years. This is shown in Figure 36. At the beginning the model was set to run in a time interval of 24 years, but it was decided to extend this prediction strategy ten more years in order to further understand the extent of the CO_2 plume behavior near the zone of the producer well ***(PROD).***

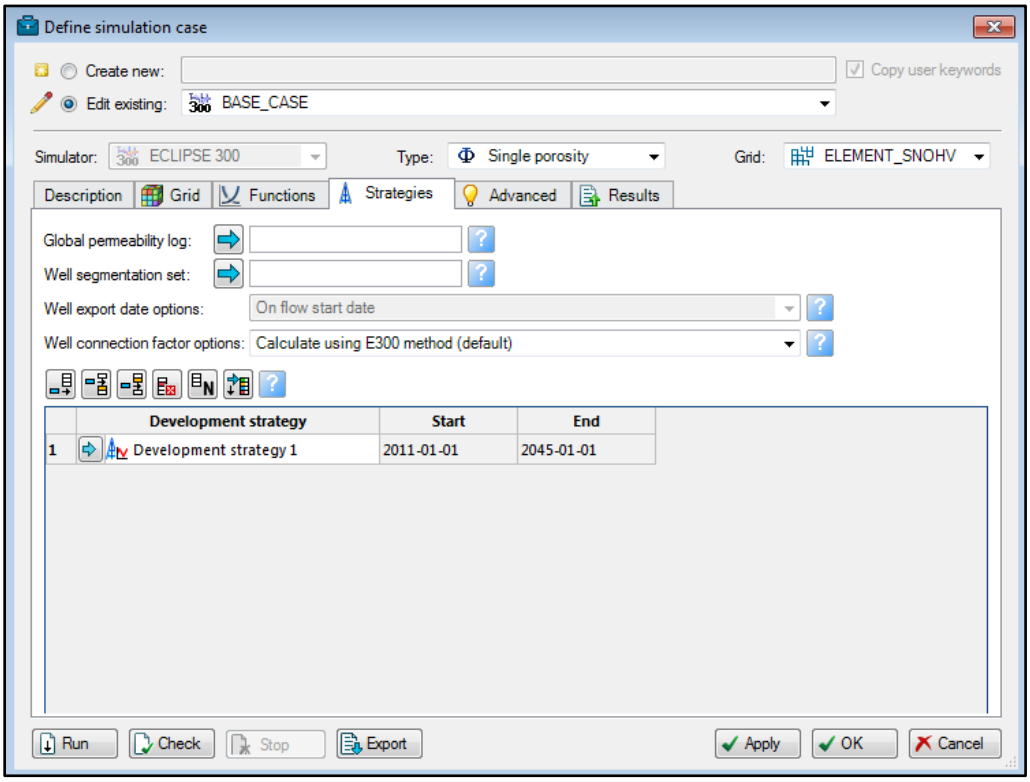

Figure 36. Development Strategy established for the segment model or BASE_CASE

5.0 RESULTS

The conditions stated in the last chapter were taken into account in this last run. As mentioned, the production rate restriction was lowered, and established at 50 Sm^3/day.

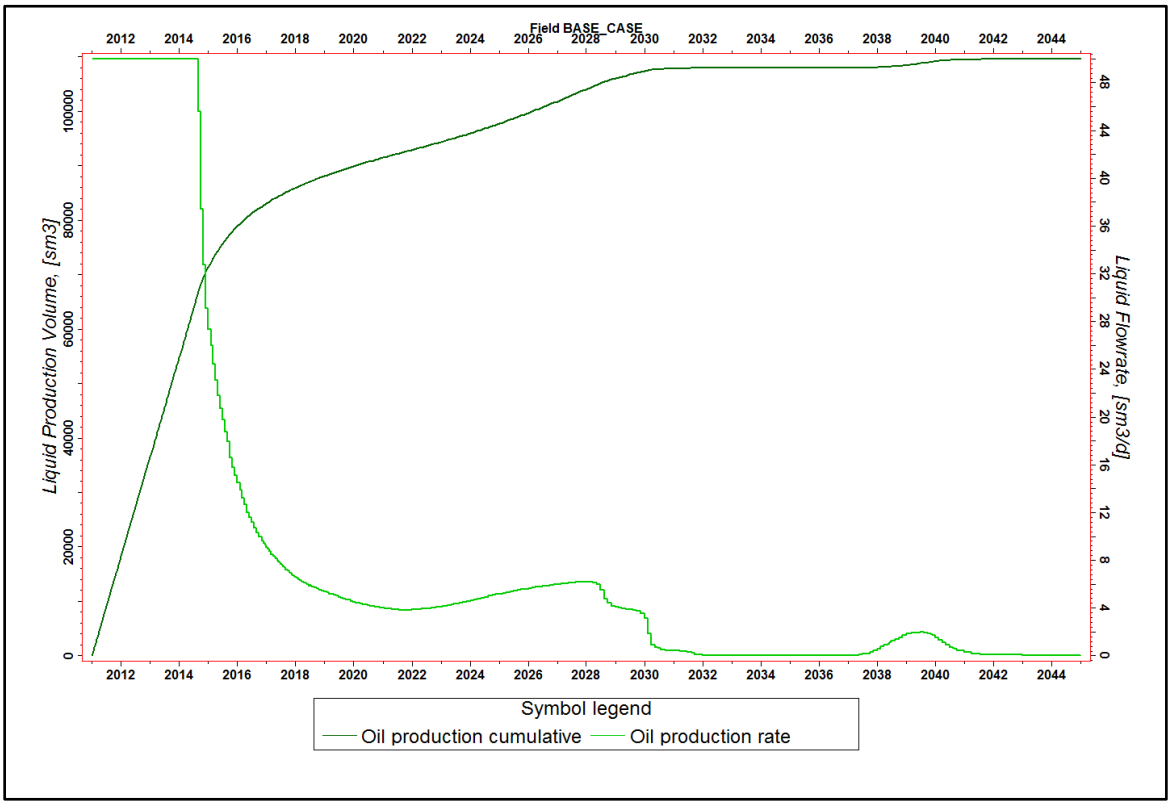

Figure 37. Cumulative Oil Production & Oil Production Rate

As can be seen in Figure 37, the oil production cumulative is exemplified in dark green color and the oil production rate in a lighter green color. The horizontal axis shows the time in years, the left axis shows the liquid production volume in Sm^3 and the right-hand axis shows the liquid flow rate in Sm^3 per day.

The cumulative oil production at the end of 34 years was of nearly 110.000 Sm^3 of total liquid volume. The oil production rate was met stable during the first three years until the middle of 2014 where it started to reduce steadily, nonetheless at the beginning of 2017 the daily oil production was already near 10 Sm^3/day. In the next 12 years it would be maintained between 4 Sm^3/day and 8 Sm^3/day until the middle of 2030 where the rate would decrease to values between 0.5 and 2 Sm^3/day. It is notable to highlight that in 2030 a cumulative production of 100.000 Sm^3 (0.1 million

Sm^3) is reached and it can be a variable taken into to account in order to continue the production or stop the operation and just remain with injection and subsequent storage of CO_2.

Analyzing Figure 38, the water cumulative production is shown as a line in a dark blue color and the water production rate as a line in orange. The horizontal axis is time in years, the left-hand axis shows the liquid flow rate in Sm^3 per day and the right-side axis shows the liquid volume production in Sm^3. Bearing in mind what was mentioned in the last paragraph, it is possible to identify that there is no water production during the first three years of oil production, which is a promising scenario in view of improved oil recovery. And can be counted as an enhancement to other earlier runs, where the production restriction values which were set first at 500 Sm^3/day and the production control rate was constant during the first few months but then it would drastically drop to values ranging between 3 and 4 Sm^3/day.

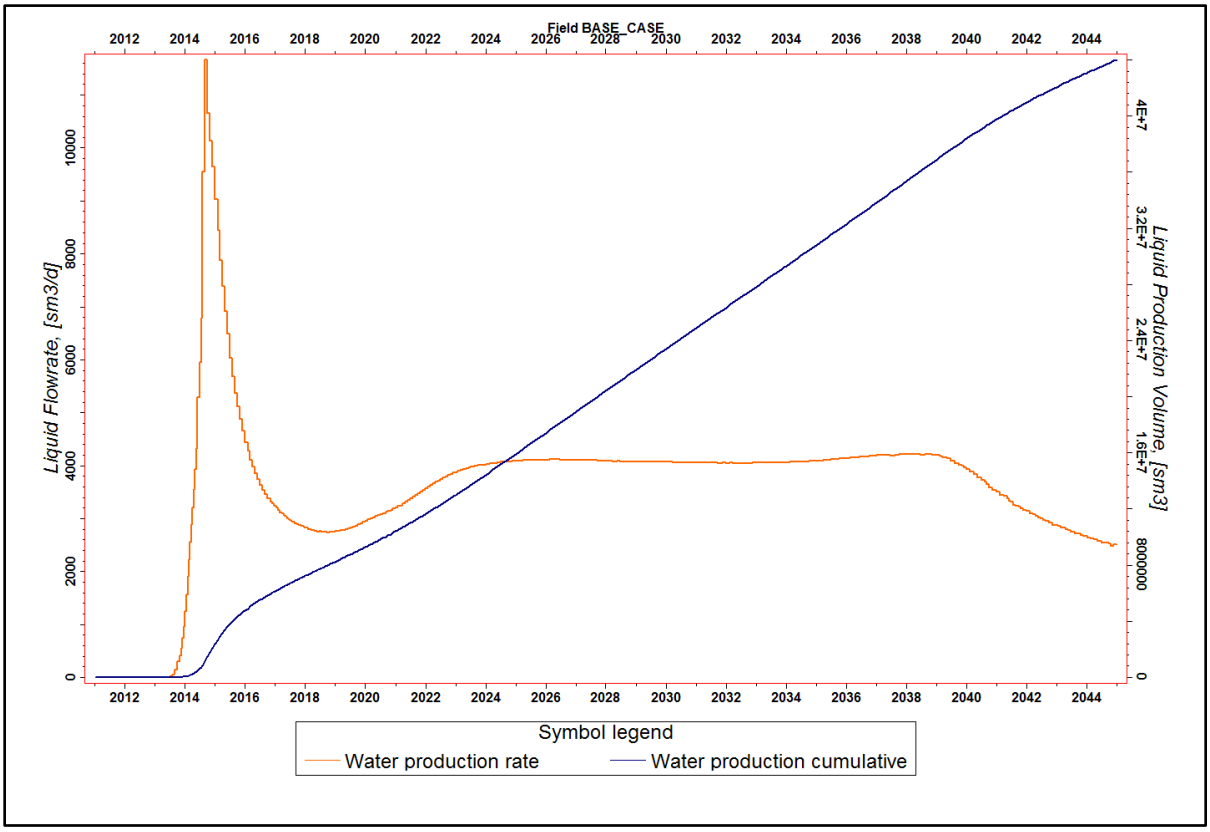

Figure 38. Cumulative Water Production & Water Production Rate

The water production rate meets a maximum value of 12.000 Sm^3/day around 2014, coinciding with the date the production rate of oil starts to decrease, then in 2018 it drops to a minimum value

of 2700 Sm^3/day and finally it increases until where it is maintained somewhat constant at 4000 Sm^3/day until the year 2040 and lastly starts to decrease until the end of the life of the field in study. The cumulative water production ended with a total value of 44 MSm^3.

In Figure 39 the Cumulative Gas Production and the gas production rate are presented as red and purple lines, respectively. The horizontal axis presents the time in years, the left axis represents the gas production volume in Sm^3 and the right-side axis shows the gas volume rate in Sm^3 per day. For the gas production rate, it is important to note that during the first three years, the parameter is maintained steadily constant at around 2.2 MSm^3/day but around the time that the oil production rate starts to decrease (Figure 37), the gas rate shows an increment, much like the situation that develops with the water production rate (Figure 38). In this case the maximum value for the gas production rate is of 3 MSm^3/day. In 2022 it reaches a minimum value of 350.000 Sm^3/day, but then it would increase and be maintained in around 400.000 Sm^3/day and in 2040 it would increase to have a last value of close to 900.000 Sm^3/day.

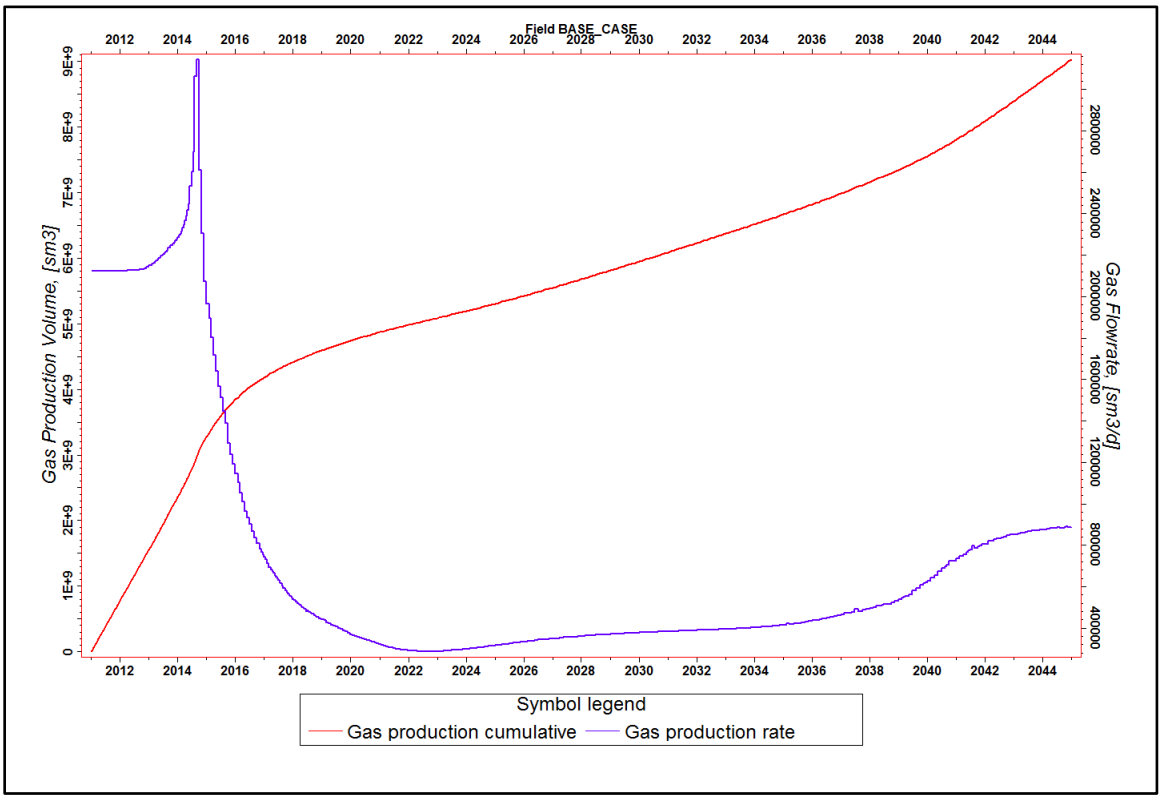

Figure 39. Cumulative Gas Production & Gas Production Rate

The cumulative gas production ends with a total value of 9000 MSm^3 in the year 2045.

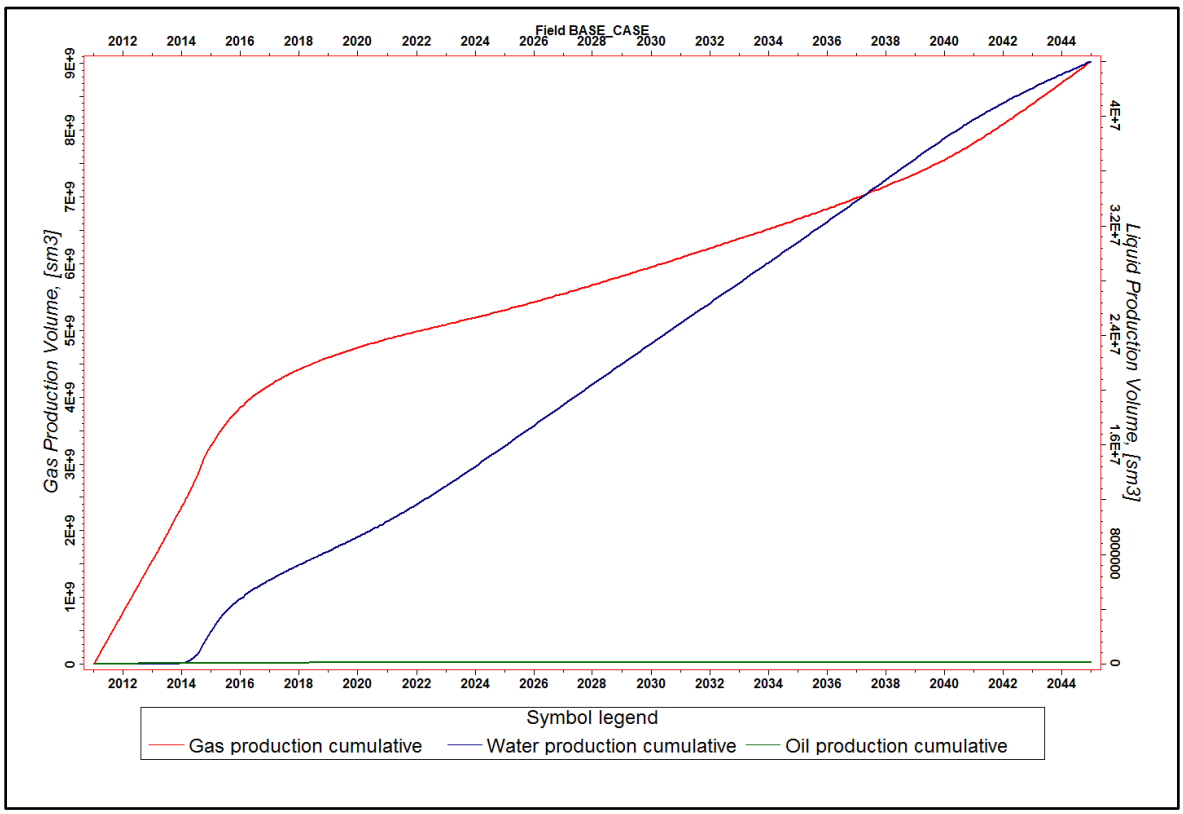

Figure 40. Cumulative Oil, Gas & Water Production

As can be seen from Figure 40, the cumulative production for all the phases present in the reservoir is displayed. Oil is shown in green, water in blue and gas in red colors. The horizontal axis is the time in years, the left-side axis is the gas production volume in Sm^3 and the right-side axis the liquid production volume in Sm^3 as well. It is important to highlight that regardless of the behavior of the curve pertaining cumulative oil production which seems to be nearly zero, this is not the case. The variable appears to have this behavior because compared to the high volumes of gas and water retrieved, it seems as if the values of oil where non-existent. It is also possible to state that in Sm^3 volumes of liquid, much more gas is produced because Snøhvit is a gas reservoir. And a high volume of water is retrieved because the whole operation is taken place in the water bearing zone of the Stø formation.

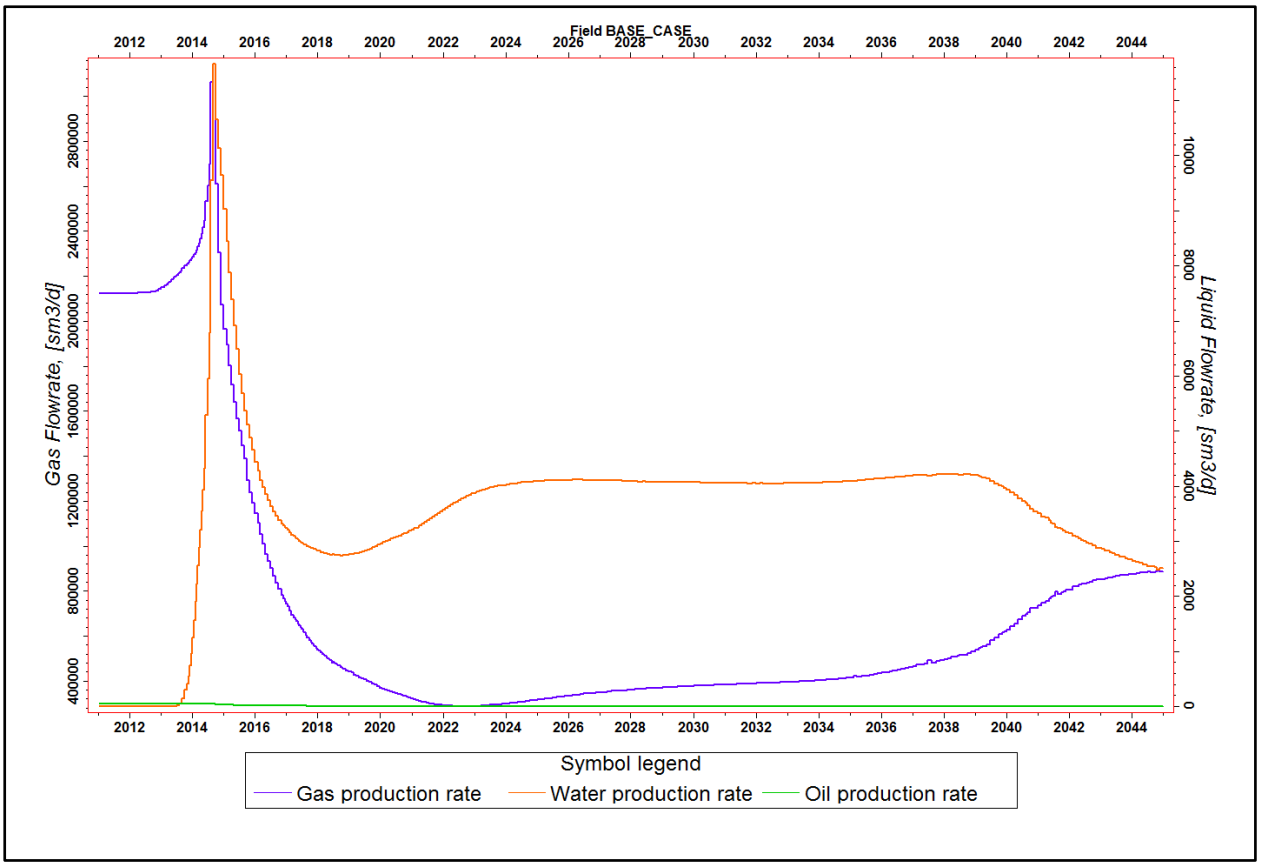

Figure 41. Oil, Gas & Water Production Rate

On Figure 41, the production rate of all of the phases is shown in Sm^3/day. Gas is shown as blue, water as orange and oil as green color lines. The horizontal axis is the time in years, the left-side axis is the gas flow rate in Sm^3 per day and the right-side axis the liquid flow rate in Sm^3 per day.

A familiar development to the curves of Figure 40 is shown, taking into account that the oil production rate seems to be close to zero. This is a phenomenon of the scales that are being used in the axes, which have to account for high flow rates for the water and gas phases, compared to the flow rates of oil. After the year 2022 the gas production curve seems to reach a constant value, but somewhere around 2024, as the production of water is maintained at a somewhat constant rate and the production of oil shows a slight increase (keeping in mind the development in Figure 37), the gas production increases towards the end of the prediction made in the segment model. The producer well would start to deliver high amounts of gas and some amount of condensate from the formation, with a considerable high water cut.

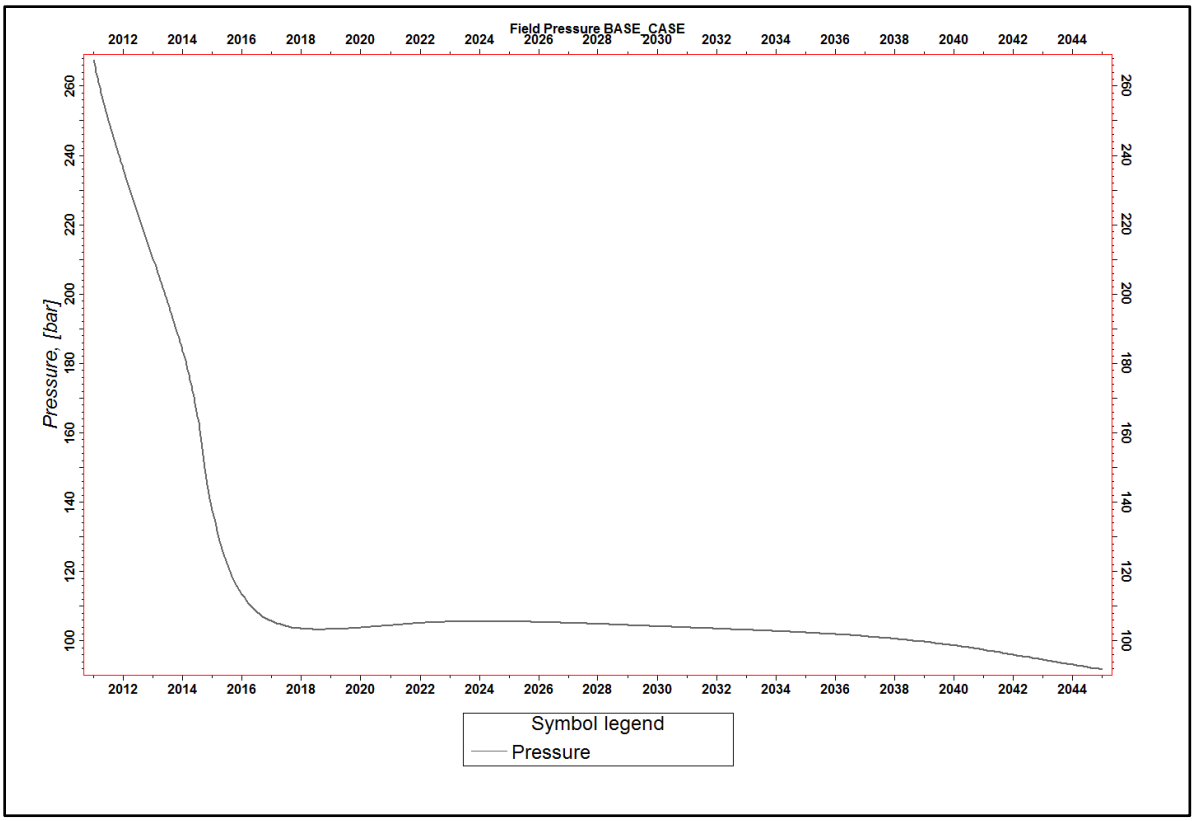

Figure 42. Pressure Development BASE_CASE

The pressure development is presented in Figure 42, where the horizontal axis is the time in years and the left-hand axis shows the pressure in bars. The base case seems to start at pressures close to 280 bars and next it diminishes from 2011 to 2016 where it reaches a minimum value of 105 bars but then increases and stays at an average value of 110 bars until the year 2037 where it begins to reduce more rapidly until the year 2045 when the pressure value is close to 100 bars.

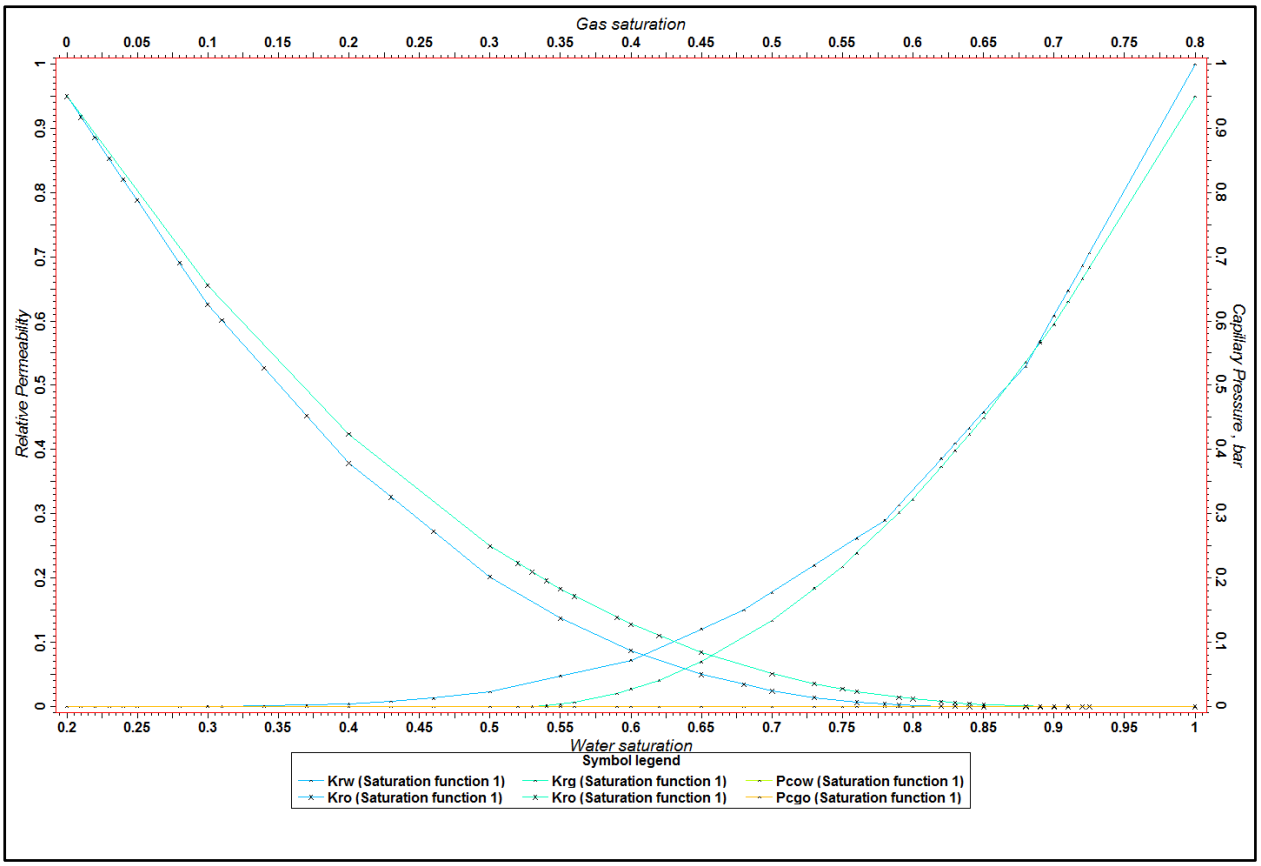

Figure 43. Relative Permeabilities BASE_CASE

The relative permeabilities can be shown in Figure 43. The lower horizontal axis reflects water saturation, and the upper horizontal axis shows gas saturation. The left-hand axis shows the values for the relative permeabilities and the right-hand axis presents the capillary pressure. The saturation value at which K_{rw} and K_{ro} are equal, i.e. the point of intersection between the curves, together with the end points of K_{ro} and K_{rw}, is related to the wet condition of the rock. Therefore, it is advisable to validate this point with the result of the wettability test.

The behavior of the permeability curves relative to gas and oil has a normal result. The main differences are: Due to the differences in viscosities between the oil and the gas, the breaking point occurs very early. The non-wetting phase is represented by the gas and the wetting phase by oil.

The curves are monotonous and non-linear. For homogeneous samples the curves are smooth. The Kro curve always decreases with S_w, while K_{rw} is always increasing.

An important characteristic of the curves of relative permeabilities is the value of K_{rw} in situation of S_{or}, which in the graph is referred to as "end point of K_{rw}". The value of this point is used as an indicator of the wettability of the rock-fluid system. As with the saturation of residual oil, special attention must be given in the treatment of this final point, since it is a critical value used in reservoir simulations. For example, the value of S_{or} could be very high as a consequence of the premature completion of the displacement, so that the end point of K_{rw} is very low. The results of relative's curves in this case don't show such situation.

The BASE_CASE segment model is seen in Figure 44 presenting gas saturation, being the red value 100% gas saturation and the violet color 0% gas saturation. A lot of oil is produced in the form of gas condensate, which is why the gas saturation is used as reference. As aforementioned in Chapter 4, the injector is located directly above a zone that is 100% water, henceforth making the violet area, an area covered and comprised by water.

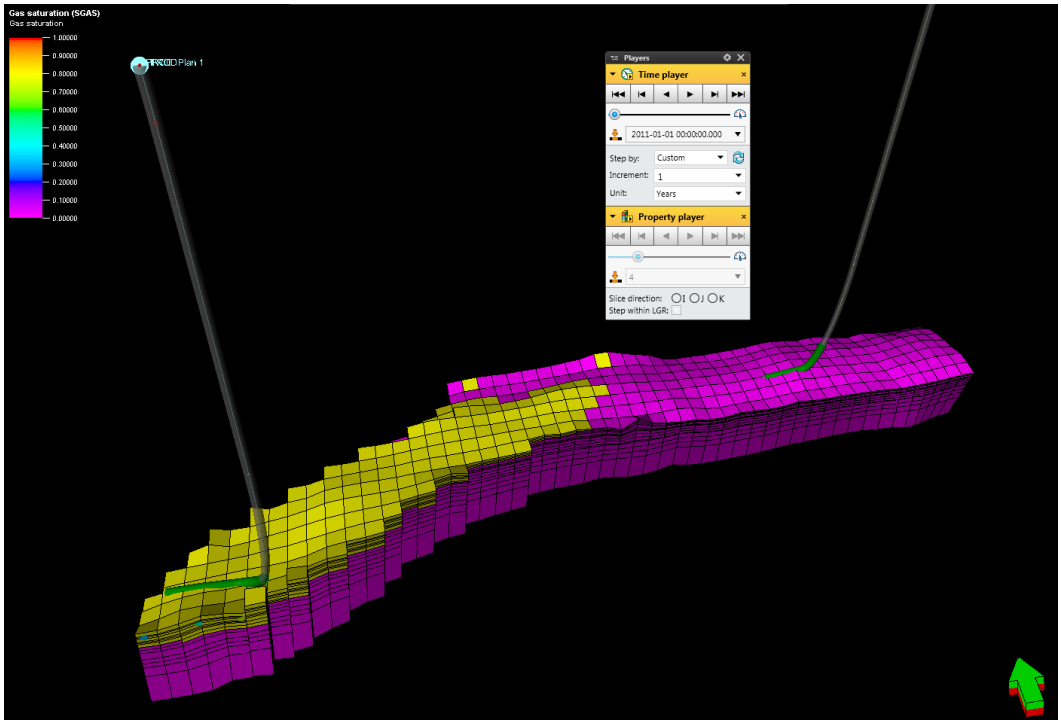

Figure 44. Gas Saturation at initial time for BASE_CASE

The gas saturation in a large portion of the segment, closer to the producer well, has a value of 80%, which is an important percentage to keep in mind. The gas is not only shallow in the upper property layer acting as a gas cap, but is also distributed in lower layers of the BASE_CASE model.

In the following images it can be seen how the gas saturation is evolving in the segment model through time. The time and property layer option have been selected in the player designated to run for 34 years of simulation in Petrel 2018. As seen in Figure 45, the property layer 6 was chosen in order to show a better understanding on how the hydrocarbon phase reacts when contacted with the injected CO_2 plume. Starting from 2011 (Figure 45a), the saturation of CO_2 around the injector is zero percent because injection has not begun yet, and around the producer it shows values of 80% gas saturation in some areas. Then focusing in 2017 (Figure 45b), it is possible to witness that the gas saturation around the injector has a value that ranges from 0.5 and 0.6 (50-60%). Whereas the gas saturation near the producer well remains to have lowered, having values to go from 0.3 to 0.5 (30-50%). Nonetheless, the area covered by gas near the producer seems to have increased slightly.

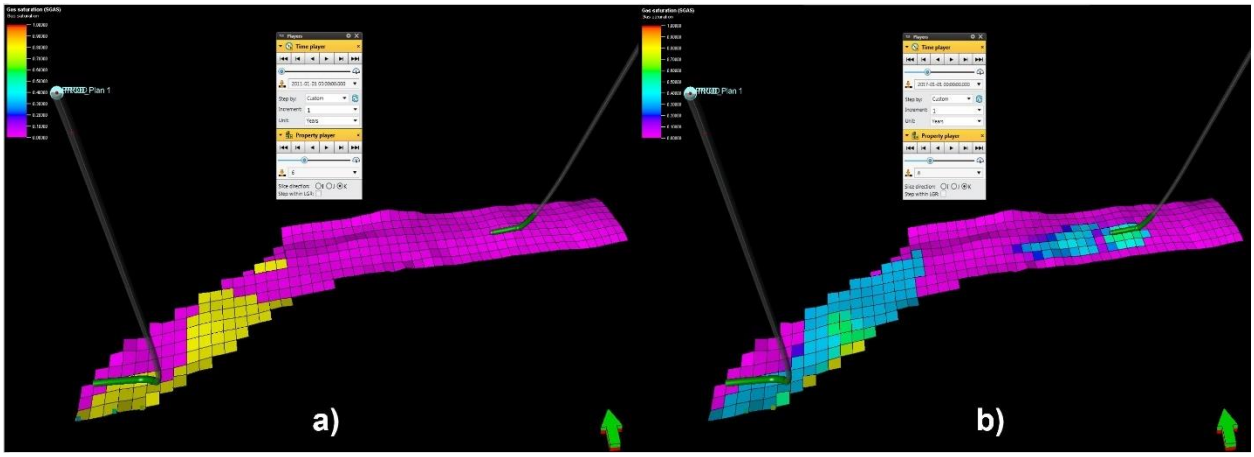

Figure 45. Gas Saturation at a) 2011 & b) 2017

More after, Figure 46a) showcases the gas saturation in the year 2020, and it can be visualized how the CO_2 plume has started to migrate and to contact the hydrocarbon phase of the segment model. The saturations near the producer are close to 40% of gas, and it can be assumed that the lighter components of the upper layers have started to be produced.

By the year 2025 (Figure 46b) a great part of the CO_2 plume has contacted the hydrocarbon phase close to the producer, nearly displacing it all and saturating the portion left behind with carbon dioxide, as presented below.

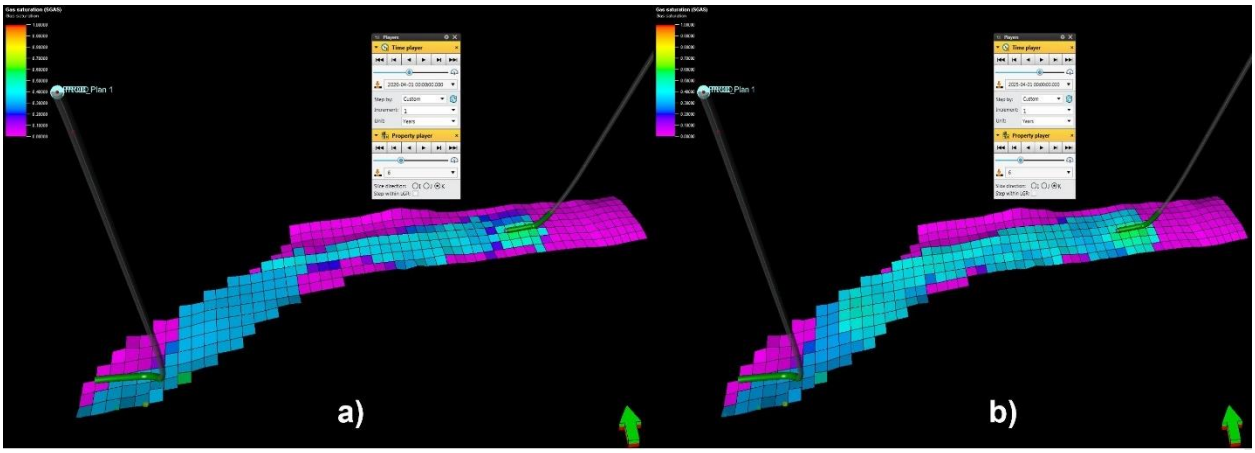

Figure 46. Gas Saturation at a) 2020 & b) 2025

In figure 47a), it is the year 2035 and it can be safely said that a great percentage of the hydrocarbon phase has been produced, including the gas and oil in the form of condensate. Therefore, breakthrough of CO_2 should have already taken place around this time. In figure 47b) it is the last year of the prediction run, 2045, and the gas saturation of CO_2 near the producer has increased to values close to 60%.

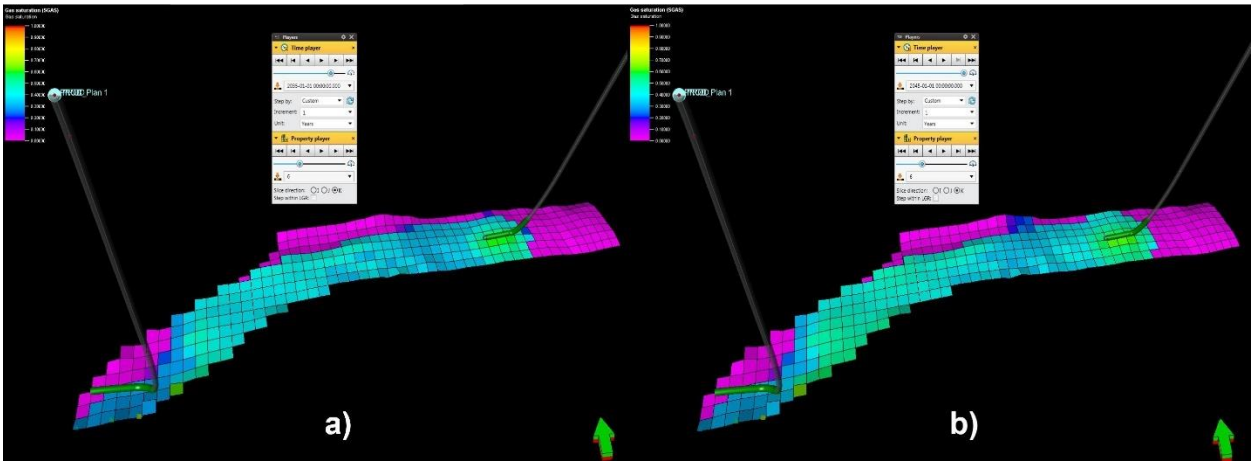

Figure 47. Gas Saturation at a) 2035 & b) 2045

In the prediction analysis done before, the property layer 6 was the one taken into account. The permeabilities of each property layer are shown in Figure 48. If looking into the permeability ranges, it is possible to note that layers 4 to 6 have permeabilities close to 10 mD. And the layers from number 7 to number 9 have a permeability value close to 1000 mD, which demonstrates that this petrophysical property of the rocks is good and the fluid injected can move much more freely contacting more areas in the horizontal direction.

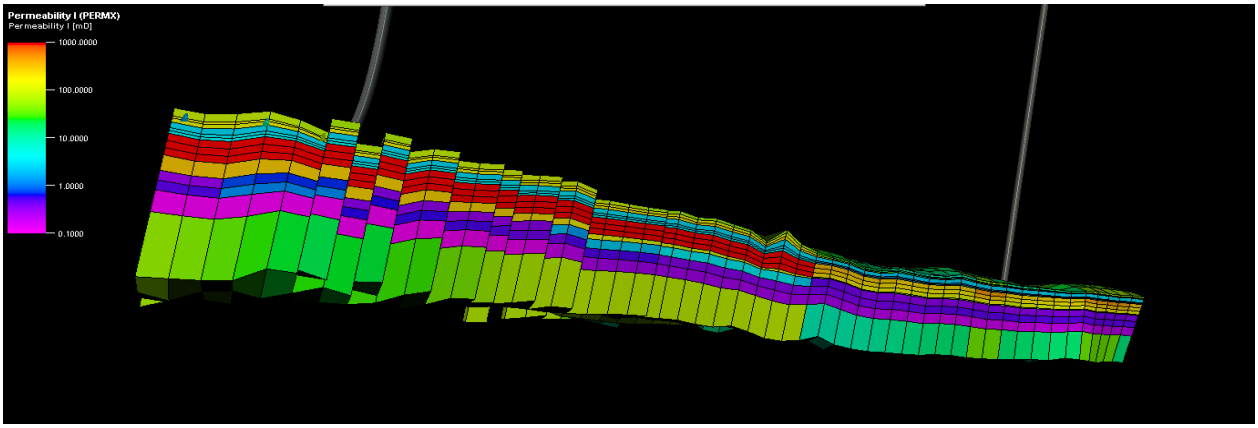

Figure 48. Permeabilities in each of the property layers (PERMX)

6.0 CONCLUSIONS

- For the prediction of the segment model, the CO_2 plume dissolves in the hydrocarbon and gradually helps the oil phase (in the form of gas condensate) to be produced, only from the contact zone. Therefore, acting as CO_2 miscible flood.

- Under the conditions settled in the model, the recoverable hydrocarbon volumes are 110.000 Sm^3 of gas condensate. In surface it is in liquid phase, and it is much more valuable than natural gas, due to the presence of heavier components.

- During the first three years of the prediction, there is basically no water production, therefore allowing for a better behavior of the hydrocarbon towards the producer well. The overall water produced in the span of 34 years is of 44 MSm^3.

- In the interphase between the oil and the carbon dioxide, the intermediate and higher molecular weight hydrocarbons from the reservoir oil vaporize into the CO_2 and part of the injected CO_2 dissolves into the oil. The gas condensate is being produced by the CO_2 plume but there is no piston-effect, there is miscible flooding with the oil removed from the interphase.

7.0 RECOMMENDATIONS

- The simulation results show potential for liquid volume production of the hydrocarbon present in the small segment model from Snøhvit. Therefore, it would be viable to apply CCUS in the larger Snøhvit field, by drilling a well that is placed in the right location and operated under the proper conditions.

- Since, in the software used, each grid has a size of around 20 meters per side, it is not possible to fully comprehend the development of the fluids behavior at a smaller scale, henceforth to counter the effects of numerical diffusion a more refined spatial discretization is recommended to further understand in depth the phenomena taking place.

8.0 REFERENCE LIST

Alnes, H., Eiken, O., Nooner, S., Sasagawa, G., Stenvold, T., & Zumberge, M. (2011). Results from Sleipner gravity monitoring: Updated density and temperature distribution of the CO_2 plume. *Energy Procedia*, *4*, 5504-5511. doi: 10.1016/j.egypro.2011.02.536

Bachu, S., and Adams, J. (2003). Sequestration of CO_2 in geological media in response to climate change: capacity of deep saline aquifers to sequester CO_2 in solution. Energy Conversion and Management, 44(20), p. 3151-3175.

Bardon, C., & Denoyelle, L. (1984). CO_2 Injection to Enhance Heavy Oil Recovery. Heavy Crude Oil Recovery, p. 177-209.

Beecher, C. E., & Parkhurst, I. P. (1926). Effect of Dissolved Gas upon the Viscosity and Surface Tension of Crude Oil. Society of Petroleum Engineers.

Bernard G.G., Holm L.W. and Harvey, C.P. (1980). Use of Surfactant to Reduce CO_2 Mobility Control. SPEJ p. 281-292.

Bryant, D.W. and Monger, T.G. (1985). Multiple Contact Phase Behaviour Measurement and Application Using Mixtures of Carbon Dioxide and Highly Asphaltic Crude. SPE Paper 14150.

Carr, N.L, Kobayashi, R. and Burrows D.B. (1959). Viscosity of Hydrocarbon Gases Under Pressure. p. 264-272.

CO_2 trapping mechanisms – CO_2 Capture project (2019). Retrieved from https://www.co2captureproject.org/co2_trapping.html

Chung, F.T. and Burchfield, T.E. (1987), Research Aimed at Immiscible CO_2 Flooding. *Oil and Gas Journal*, p. 76-82.

Dodds, W.S., Stutzman, L.F., and Sollami, B.J. (1956). Carbon Dioxide Solubility in Water, p. 92-94.

Eiken, O., Ringrose, P., Hermanrud, C., Nazarian, B., Torp, T., & Høier, L. (2011). Lessons learned from 14 years of CCS operations: Sleipner, In Salah and Snøhvit. *Energy Procedia, 4*, 5541-5548. doi: 10.1016/j.egypro.2011.02.541

Ellis, A.J. (1959). The Solubility of Calcite in Carbon Dioxide Solution. *Am. J. Sci*. p. 354-365.

Farouq Ali, S.M. (1992). *Oil Recovery by Carbon Dioxide*. Edmonton: The University of Alberta.

Farouq Ali, S.M. and Rojas G. (1985a). Dynamics of Subcritical Brine C/Brine Floods for Heavy Oil Recovery. *Society of Petroleum Engineers*.

Farouq Ali, S.M. and Rojas G. (1985b). Current Technology of Heavy Oil Recovery by Immiscible Carbon Dioxide and Water-flooding. Third International Conference of Heavy Crude Oil and Tar Sans. Puerto La Cruz, Venezuela.

Farouq Ali, S.M, Thomas, S. and Khambaratana, F. (1988). Formation and Flow of Emulsions in Porous Media. AOSTRA 493. The Final Report. The University of Alberta.

Goodrich, J.H. (1980). Review and Analysis of past and Ongoing Carbon Dioxide Injection Field Tests. *SPE/DOE* 8832.

Halland, E.K., Mujezinovic, J. and Riis F. (Eds) (2014). *CO_2 Storage Atlas: The Barents Sea*. Norwegian Petroleum Directorate, Stavanger.

Hansen, O., Gilding, D., Nazarian, B., Osdal, B., Ringrose, P., & Kristoffersen, J. et al. (2013). Snøhvit: The History of Injecting and Storing 1 Mt CO_2 in the Fluvial Tubåen Fm. *Energy Procedia*, *37*, 3565-3573. doi: 10.1016/j.egypro.2013.06.249

Hermanrud, C., Andresen, T., Eiken, O., Hansen, H., Janbu, A., & Lippard, J. et al. (2009). Storage of CO_2 in saline aquifers–Lessons learned from 10 years of injection into the Utsira Formation in the Sleipner area. *Energy Procedia*, *1*(1), 1997-2004. doi: 10.1016/j.egypro.2009.01.260

Hermanrud, C., Halkjelsvik, M. E., Kristiansen, K., Bernal, A., & Strömbäck, A. C. (2014). Petroleum column-height controls in the western Hammerfest Basin, Barents Sea. *Petroleum Geoscience*.

Hirschberg, A. deJong, L.N., Schipper, B.A, and Meijers, J.G. (1981). Influence of Temperature and Pressure on Asphaltene Flocculation. p. 283-291.

Holm, L., & Josendal, V. (1974). Mechanisms of Oil Displacement by Carbon Dioxide. *Journal of Petroleum Technology*, 26(12), p. 1427-1438.

Jacobs, F.A. (1978). *Viscosity of Carbon Dioxide Saturated Athabasca Bitumen*. MSc Thesis. University of Calgary.

Jarrell, P.M., Fox, C.E., Stein, M.H., nad Webb, S.L. (2002). Practical Aspects of CO_2 flooding, *Society of Petroleum Engineers Monograph Series*, p. 220.

Kaufmann, R., Skurtveit, E. (Eds) (2018) *"Snøhvit: A success story".* FME SUCCESS publication, p. 10.

Killesreiter, H. (1982). Competing Effect of Temperature and Dissolved Gas on the Viscosity of Petroleum. *Erdol Kohle Erdgas Petrochem*. p. 428-431.

Klins, M. (1984). Carbon dioxide flooding: Basic Mechanisms and Project Design. *HRDC*, Boston.

Larsen, J. W. (2004). The effects of dissolved CO_2 on coal structure and properties. International Journal of Coal Geology, 57, p. 63-70.

Lashkarbolooki, M., Eftekhari, M., Najimi, S., & Ayatollahi, S. (2017). Minimum miscibility pressure of CO_2 and crude oil during CO_2 injection in the reservoir. *The Journal of Supercritical Fluids*,127, 121-128.

Law, D., & Bachu, S. (1996). Hydrogeological and numerical analysis of CO_2 disposal in deep aquifers in the Alberta sedimentary basin. Energy Conversion and Management, 37(6-8), p. 1167-1174.

Lund, K. and Fogler, H.S. (1976) Acidization V, The Prediction of the Movement of Acid and Permeability Fronts in Sandstone. *Chem. Eng. Sci*., p. 381-392.

Martin, J.W. (1951). Additional Oil Production Through Flooding with Carbonated Water. *Producers Monthly*, Vol. 15.

Metz, B. (2005). IPCC special report on carbon dioxide capture and storage. *Cambridge: Published for the Intergovernmental Panel on Climate Change, Cambridge University Press*, Technical Summary.

McPherson, Brian, and Barret Cole, (2000). Sequestration of CO_2 in the Powder River Basin, Wyoming. AAPG Bulletin, p. 84.

Module 5 CO_2 storage options and trapping mechanisms | Global CCS Institute. (2019). Retrieved from https://hub.globalccsinstitute.com/publications/building-capacity-co2-capture-and-storage-apec-region-training-manual-policy-makers-and-practitioners/module-5-co2-storage-options-and-trapping-mechanisms

Nooner, S., Eiken, O., Hermanrud, C., Sasagawa, G., Stenvold, T., & Zumberge, M. (2007). Constraints on the in-situ density of CO_2 within the Utsira formation from time-lapse seafloor

gravity measurements. *International Journal of Greenhouse Gas Control*, *1*(2), 198-214. doi: 10.1016/s1750-5836(07)00018-7

Norwegian Petroleum Directorate, 2018,<http://factpages.npd.no/ReportServer?/FactPages/PageView/field&rs:Command=Render&rc:Toolbar=false&rc:Parameters=f&NpdId=2053062&IpAddress=213.236.242.137&CultureCode=en>.

Oyekan, R. (1983), *Analysis of Carbon Dioxide Recovery of Residual Oil Using a Linear Scaled Model*. PhD Dissertation. University of Southern California.

Page, B. (2018). CCS: A solution to climate change right beneath our feet [Email]

Pawar, R., Bromhal, G., Carey, J., Foxall, W., Korre, A., & Ringrose, P. et al. (2015). Recent advances in risk assessment and risk management of geologic CO_2 storage. *International Journal of Greenhouse Gas Control*, *40*, 292-311. doi: 10.1016/j.ijggc.2015.06.014

Ringrose, P. (2018). The CCS hub in Norway: some insights from 22 years of saline aquifer storage. *Energy Procedia*, *146*, 166-172. doi: 10.1016/j.egypro.2018.07.021

Ringrose, P., Roberts, D., Gibson-Poole, C., Bond, C., Wightman, R., & Taylor, M. et al. (2011). Characterisation of the Krechba CO_2 storage site: Critical elements controlling injection performance. *Energy Procedia*, *4*, 4672-4679. doi: 10.1016/j.egypro.2011.02.428

Ritchie, H. and Roser, M. CO_2 and other greenhouse gas emissions (2017). Retrieved from https://ourworldindata.org/co2-and-other-greenhouse-gas-emissions

Rojas, G. (1985). *Scaled Model Studies of Immiscible Carbon Dioxide Displacement in Heavy Oil*. PhD Thesis. The University of Alberta.

Ross, G.D, Todd A.C., Tweedie, J.A., and Will, A.G.S. (1981). The dissolution Effects of CO_2 Brine Systems on the Permeability of U.K. and North Sea calcareous sandstones. SPE Paper 10685.

Savegh S.G. and Maini, B.B. (1984), Laboratory Studies of the CO_2 Huff-N-Puff Process for Heavy Oil Reservoirs, p. 29-36.

Saxon, J. Jr., Breston J.N., and Macfarlane, R.M (1951) Laboratory tests with Carbon Dioxide and Carbonated Water as Flooding Mediums, p. 8-14.

Shi, J., Imrie, C., Sinayuc, C., Durucan, S., Korre, A., & Eiken, O. (2013). Snøhvit CO_2 Storage Project: Assessment of CO_2 Injection Performance Through History Matching of the Injection Well Pressure Over a 32-months Period. *Energy Procedia*, *37*, 3267-3274. doi: 10.1016/j.egypro.2013.06.214

Simon, R., & Graue, D. (1965). Generalized Correlations for Predicting Solubility, Swelling and Viscosity Behavior of CO_2 -Crude Oil Systems. *Journal of Petroleum Technology*,17(01), p. 102-106.

Stalkup F. (1984). Miscible Displacement: Dallas, Tex., *Society of Petroleum Engineers of AIME, SPE Monograph Series*, ISBN 0-89520-319-7, p.204.

Stalkup, F. (1983). Status of Miscible Displacement. *Journal of Petroleum Technology*, *35*(04), 815-826.

Van Poolen, H.K., and Associates (1981). Fundamentals of enhanced oil recovery. *Penn Well Books*, p 155.

Stewart, P.B, and Munjal, P. (1970). Solubility of Carbon Dioxide in Pure Water, Synthetic Sea Water, and Synthetic Sea Water Concentrates at -5 C to 25 C and 10 to 45 atm. *Chemical Engineering Data Series*, p. 92-94.

Syed, A., Durucan, S., Shi, J., & Korre, A. (2013). Flue Gas Injection for CO_2 Storage and Enhanced Coalbed Methane Recovery: Mixed Gas Sorption and Swelling Characteristics of Coals. Energy Procedia, p. 37.

Verma, M.K., 2015, Fundamentals of carbon dioxide-enhanced oil recovery (CO_2-EOR) ---A supporting document of the assessment methodology for hydrocarbon recovery using CO_2-EOR associated with carbon sequestration: *US. Geological Survey Open-File Report 2015-1071*.

Warner H.R. (1977). An Evaluation of Miscible Carbon Dioxide Flooding in Waterflooded Sandstone Reservoirs. *Journal of Petroleum Technology*, p. 1339-1347.

Welker, J.R., and Dunlop, D.D. (1963). Physical properties of carbonated oils, *Journal of Petroleum Technology*, p. 873.

Wildenborg, T., Chadwick, A., Deflandre, J., Eiken, O., Mathieson, A., & Metcalfe, R. et al. (2013). Key Messages from Active CO_2 Storage Sites. *Energy Procedia*, *37*, 6317-6325. doi: 10.1016/j.egypro.2013.06.560

Wildenborg, T., Chadwick, A., Deflandre, J., Eiken, O., Mathieson, A., & Metcalfe, R. et al. (2013). Key Messages from Active CO_2 Storage Sites. *Energy Procedia*, *37*, 6317-6325. doi: 10.1016/j.egypro.2013.06.560

Yellig, W., & Metcalfe, R. (1980). Determination and Prediction of CO_2 Minimum Miscibility Pressures (includes associated paper 8876). *Journal of Petroleum Technology*, *32*(01).

Zhu, T. (1986), *Displacement of a Heavy Oil by Carbon Dioxide and Nitrogen in a Scaled Model*, MSc Thesis. The University of Alberta.